Surface Science
and Technology

REVIEW

Open Access

High-speed atomic force microscopy in ultra-precision surface machining and measurement: challenges, solutions and opportunities

Chen Yang[1], Chao-Qun Dang[1], Wu-Le Zhu[2] and Bing-Feng Ju[2*]

Abstract

The atomic force microscope (AFM) possesses a unique capability for three-dimensional, high-resolution imaging down to the atomic level. It operates without the needs of additional requirements on sample material and environment, making it highly valuable for surface measurements. Recent advancements have further transformed AFM into a precision machining tool, thanks to its exceptional force measurement capability and positioning precision. High-speed AFM (HS-AFM) is a specialized branch of AFM that inherits the advantages of high spatial resolution of typical AFM but with significantly improved time resolution down to the sub-second level. In this article, instead of delving into extensive research progress enabled by HS-AFM in the broad fields of biology, biophysics, and materials science, we narrow our focus to the specific applications in the domain of ultra-precision surface machining and measurement. To the best of the authors' knowledge, a comprehensive and systematic summary of the contributions that HS-AFM brings to this field is still lacking. This gap could potentially result in an underappreciation of its revolutionary capabilities. In light of this, we start from an overview of the primary operating modes of AFM, followed by a detailed analysis of the challenges that impose limitations on operational speed. Building upon these insights, we summarize solutions that enable high-speed operation in AFM. Furthermore, we explore a range of applications where HS-AFM has demonstrated its transformative capabilities. These include tip-based lithography (TBL), high-throughput metrology, and in-line inspection of nanofabrication processes. Lastly, this article discusses future research directions in HS-AFM, with a dedicated focus on propelling it beyond the boundaries of the laboratory and facilitating its widespread adoption in real-world applications.

Keywords High-speed atomic force microscopy, Ultra-precision surface machining, High-throughput metrology, Nanofabrication

1 Introduction

The atomic force microscope (AFM) is a powerful tool that enables three-dimensional (3D) imaging, modifying and manipulating the sample surface down to the atomic level. Originally invented by Binning et al. [1] in 1986, AFM was soon utilized as a versatile imaging tool for atomic and molecular analyses. In the context of ultra-precision surface measurement, AFM exhibits three significant advantages over electron beam and optical measurement methods. First and foremost, AFM

*Correspondence:
Bing-Feng Ju
mbfju@zju.edu.cn
[1] ZJU-Hangzhou Global Scientific and Technological Innovation Center, Zhejiang University, Hangzhou, China
[2] State Key Laboratory of Fluid Power Transmission and Control, Zhejiang University, Hangzhou, China

© The Author(s) 2023. **Open Access** This article is licensed under a Creative Commons Attribution 4.0 International License, which permits use, sharing, adaptation, distribution and reproduction in any medium or format, as long as you give appropriate credit to the original author(s) and the source, provide a link to the Creative Commons licence, and indicate if changes were made. The images or other third party material in this article are included in the article's Creative Commons licence, unless indicated otherwise in a credit line to the material. If material is not included in the article's Creative Commons licence and your intended use is not permitted by statutory regulation or exceeds the permitted use, you will need to obtain permission directly from the copyright holder. To view a copy of this licence, visit http://creativecommons.org/licenses/by/4.0/.

enables the acquisition of authentic 3D measurements with an exceptional sub-nanometer resolution along the vertical axis, surpassing other types of microscopes such as scanning electron microscopes (SEM) [2], optical microscopes (OM) [3] and so on [4, 5]. Secondly, unlike SEM and scanning tunneling microscopes (STM), AFM does not impose any specific material requirements on the samples being analyzed, and thus significantly broadens its applicability across a wide range of applications [6]. Lastly, AFM offers a flexible operation that does not require specific environmental conditions. It can maintain sub-nanometer measurement resolution in various environments, including air [7], liquids [8], and vacuum [9]. In contrast, SEM and transmission electron microscope (TEM) typically require a high vacuum environment for operation.

Over the past few decades, AFM has undergone a remarkable transformation from being a surface measurement tool to becoming an ultra-precision machining tool [10, 11]. This evolution can be attributed to its precise spatial positioning and exceptional force measurement capabilities [12]. A wide spectrum of applications has been reported, encompassing local oxidation [13], deposition [14], cutting [15], milling [16] and other nanoscale lithography processes [17, 18].

High-speed atomic force microscopy (HS-AFM) is a specialized branch of AFM that offers high spatial resolution together with an unprecedented sub-second time resolution [19]. This unique capability renders it exceptionally well-suited for characterizing dynamic processes [20]. Consequently, HS-AFM has emerged as a pivotal tool for structural biologists, facilitating the study and analysis of the real-time structural dynamics exhibited by biological molecules and complexes [21]. Ando and co-workers have carefully reviewed state-of-the-art HS-AFM techniques and applications in life science. The interested readers may refer to their review papers [22–24] for details.

In this work, our aim is not to reiterate what has already been reviewed in these areas. Instead, we intend to provide a concise description of the dominant operation modes of AFM and offer a system dynamics perspective to summarize the key factors that restrict the operational speed. By doing so, we aim to enable non-expert users to gain a better understanding of state-of-the-art HS-AFM techniques, including their advantages and limitations. What's more, instead of delving into extensive research progress made in the broad fields of biology, biophysics, and materials science, we narrow our focus to the specific applications of HS-AFM in the domain of ultra-precision surface machining and measurement. According to the authors' best knowledge, a comprehensive and systematic summary of the contributions that HS-AFM brings to this field is still lacking. The remarkable capabilities of HS-AFM may not yet be fully acknowledged. Furthermore, we also wish to highlight some recent breakthroughs that have the potential to facilitate the practical deployment of HS-AFM in real-world applications, such as semiconductor inspection. These advancements have the capacity to unlock new opportunities for the utilization of HS-AFM beyond the controlled environment of the laboratory.

2 AFM operating modes and speed limitations

AFM is a powerful tool that allows various types of samples to be visualized and manipulated at the nanoscale. Soon after its invention, it was realized that various technological developments would be required to address certain limitations of the instrument [25]. This has resulted in the emergence of novel imaging modes that are constantly pushing the boundaries of AFM capabilities [26]. In this section, we delve into the fundamental principles of the three most common AFM operating modes: contact mode, amplitude modulation mode, and frequency modulation mode. We then proceed to outline the primary challenges that restrict the scanning speed in these modes. For additional representative operating modes, such as multiparametric mode and multifrequency mode, we recommend interested readers to refer to [27] and [28] for more comprehensive information.

2.1 Contact mode atomic force microscopy (CM-AFM)

2.1.1 Operating principle of CM-AFM

CM-AFM is a popular operating mode where the AFM tip maintains continuous contact with the sample surface during scanning. The schematic of CM-AFM is presented in Fig. 1. As the tip scans across the surface, it experiences repulsive forces between the atoms of the tip and the sample. These forces cause the cantilever to bend, and by measuring this deflection, the topography of the sample can be determined. The cantilever is usually made of silicon or silicon nitride, and acts as a mechanical spring that responds to the forces between the tip and the sample. The detection of the cantilever's deflection can be achieved by either using a laser beam that is reflected off the back of the cantilever and onto a position-sensitive detector (PSD) [29], or by utilizing an integrated sensing element such as a piezoelectric layer [30] or a Wheatstone bridge consisting of piezoresistive elements [31]. One of the advantages of contact mode is its simplicity and ease of use. It enables high-resolution imaging of a wide range of samples. However, there are some limitations to contact mode, such as the potential for tip wear or sample damage due to the physical contact. Thus, it is important to carefully

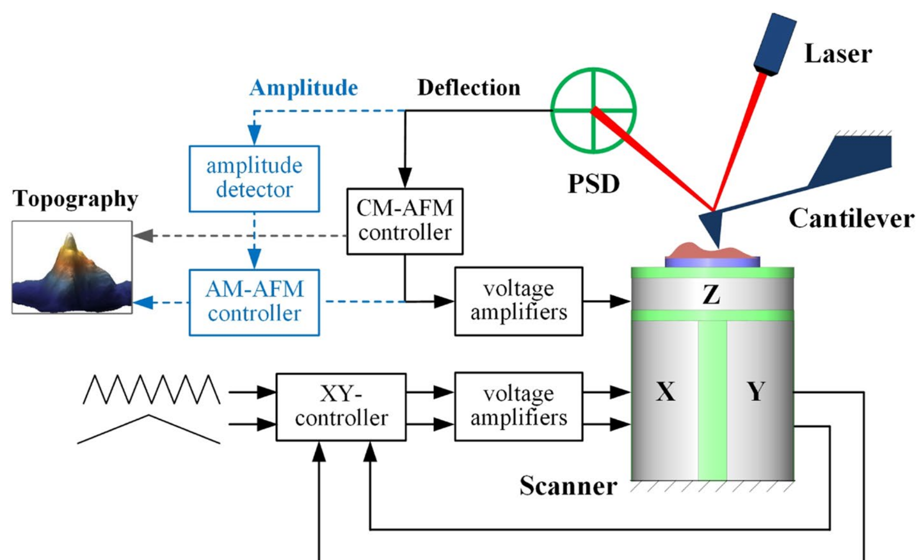

Fig. 1 Schematic of the contact mode and amplitude modulation mode. The dashed lines in blue represent the components required by AM-AFM

choose the probe and adjust the imaging parameters to ensure optimal imaging conditions.

The contact mode can be further categorized into two distinct types: constant-height contact mode and constant-force contact mode [32]. In constant height mode, the Z-scanner of the microscope maintains the AFM tip at a given height. The interaction forces between the probe and the sample cause deflection, which is then recorded and used to generate a topographic image. Constant-height contact mode is particularly useful for high-resolution imaging and characterization. However, soft samples might be destroyed by AFM tip since the exerted repulsive force is essentially uncontrollable. This issue is problematic when the sample has large topographic variations. To address the challenges associated with uncontrollable forces, the constant force mode was developed. In this mode, a feedback controller is introduced to adjust the position of the Z-scanner, ensuring that the deflection of the cantilever remains at a predetermined value. As a consequence, the repulsive force applied to the sample is maintained constant. In this mode, the displacement of the Z-scanner directly corresponds to the topography of the sample and is thus recorded and used to generate an image.

While direct contact between the AFM tip and surface may compromise accurate surface measurement and characterization, it is advantageous for tip-based manipulation [33] and fabrication [34]. Consequently, contact mode imaging is frequently favored for these particular applications.

2.1.2 Speed limitations of CM-AFM

Mathematically, the surface topography of a sample is a combination of multiple sine and cosine functions. To simplify the analysis, only the highest imaged spatial frequency was taken into account in the model of Fig. 2, which was designed to describe the interaction between a cantilever and a compliant sample, and to provide insights into the factors that limit the scan speed of CM-AFM [35, 36].

$$m\ddot{z}(t) + c\dot{z}(t) + (k + k_s)z(t) = F_0 + k_s\left(Bsin\left(\frac{2\pi\dot{x}t}{\lambda}\right)\right) \quad (1)$$

where x and z are lateral and vertical position of AFM tip; m, c and k represent the first modal mass, damping constant and stiffness of a lumped cantilever; k_s is the sample stiffness, F_0 is the external force acting on the cantilever which is independent of tip position; A and λ are the amplitude and spatial period of the sinusoidal topography. Let $\omega = 2\pi\dot{x}/\lambda$, the general solution of Eq. (1) is

$$z(t) = ce^{-\omega_0 t/2Q}sin\left(\omega_0\sqrt{1-\zeta^2}t + \varphi_1\right) + A_0(\omega)\sin(\omega t + \varphi_2) + \frac{F_0}{k + k_s} \quad (2)$$

where the resonant angular frequency, quality factor and damping ratio of the cantilever are defined as

$$\omega_0 = \sqrt{\frac{k + k_s}{m}} \quad (3)$$

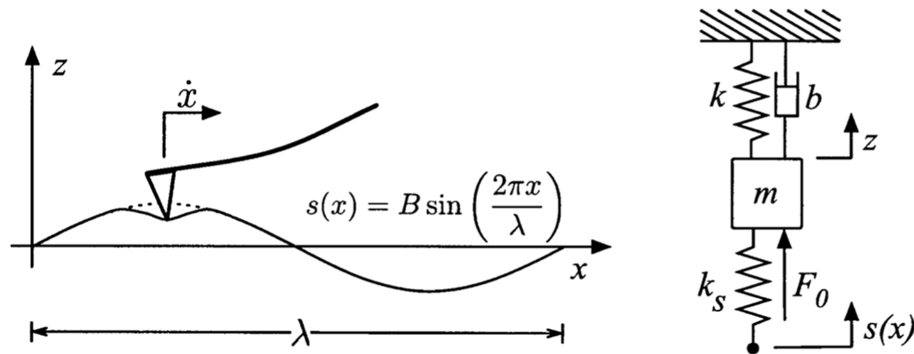

Fig. 2 Tip-sample interaction model for analyzing the speed limitation in high-speed CM-AFM [35]

$$Q = \frac{m\omega_0}{c} = \frac{m}{c}\sqrt{\frac{k + k_s}{m}} \quad (4)$$

$$\zeta = \frac{c}{2m\omega_0} \quad (5)$$

In addition,

$$\varphi_2 = acr\ tan\frac{\omega\omega_0/Q}{\omega_0^2 - \omega^2}, \quad (6)$$

$$A_0(\omega) = \frac{Bk_s/m}{\sqrt{\left(\omega_0^2 - \omega^2\right)^2 + (\omega\omega_0/Q)^2}} \quad (7)$$

In Eq. (2), the first term represents the transient response of the cantilever, while the second describes the steady-state response. The third term results from the equilibrium compression of the sample. To ensure that the response of the probe accurately reflects the topography of the sample during high-speed scanning, it is necessary to ensure that the transition time is much shorter than the steady-state sinusoidal response, i.e.,

$$\dot{x} \ll \frac{\lambda\omega_0}{2Q} \quad (8)$$

Furthermore, Eq. (7) indicates that steady-state amplitude A_0 is a function of ω, and therefore depends on the scanning speed, since $\omega = 2\pi\dot{x}/\lambda$. The amplitude thus tends to decay when ω is large, with a critical value of

$$\omega_m = \omega_0\sqrt{1 - \frac{1}{4Q^2}}. \quad (9)$$

To guarantee that the scanning speed has minimal impact on steady state imaging results, ω should be much smaller than ω_m, leading to

$$\dot{x} \ll \frac{\lambda\omega_0}{4\pi Q}\sqrt{4Q^2 - 1}. \quad (10)$$

The critical quality factor value Q_c that makes Eq. (8) and Eq. (10) equal is

$$Q_c = \sqrt{\pi^2 + 1/4}. \quad (11)$$

When $Q < Q_c$ (high damping), Eq. (10) sets the velocity constraint, whereas for $Q > Q_c$ (low damping), Eq. (8) limits the velocity.

The analysis presented above highlights two key factors for achieving high-speed CM-AFM: small quality factor and large resonant frequency of the cantilever. Additionally, it suggests that higher scanning speeds can be achieved as the stiffness of the sample increases. This observation aligns with experimental findings that high-speed scanning of hard samples tends to be much easier compared to soft samples.

2.2 Amplitude modulation AFM (AM-AFM)

2.2.1 Operating principle of AM-AFM

AM-AFM, also known as tapping mode or intermittent contact mode, involves the oscillation of a cantilever with a sharp tip near its resonance frequency [37]. In this mode, the amplitude of oscillation is typically maintained between 100–200 nm. As the tip of the cantilever gets closer to the sample surface, it encounters repulsive forces, resulting in a reduction of the oscillation.

During the scanning process, the oscillation amplitude is monitored using either an optical beam deflection system (OBD) or integrated sensing elements. The detected AC signal is then converted into a DC value by using an RMS-to-DC converter. The RMS amplitude is then compared with the predefined feedback setpoint. To minimize the error, a proportional-integral-derivative (PID) controller is usually employed. This

controller takes the error signal as input and dynamically adjusts its output proportionally, integrates the error over time, and applies derivative action to stabilize the system. The output signal from the PID controller is directed to a Z-scanner driver, which controls the displacement along vertical direction. By precisely regulating the Z scanner's displacement based on the feedback received, the error signal approaches zero. This finding suggests that the oscillation amplitude of the cantilever closely corresponds to the desired setpoint, ensuring precise and reliable surface measurements. These sequential steps are repeated at multiple locations along the scanning path while the scanner moves laterally in the XY directions. The output signal of the feedback loop is recorded at each location, allowing for the reconstruction of the sample's topography.

AM-AFM provides several advantages over CM-AFM [38]. One key benefit is the reduction of lateral forces, which is particularly advantageous for minimizing damage to soft and delicate samples during scanning. Additionally, the intermittent contact also helps to extend the lifespan of the tip by minimizing wear and tear. It is important to highlight the high sensitivity of AM-AFM to surface interactions. This sensitivity opens up possibilities for investigating various surface characteristics, such as elasticity [39], viscosity [40], adhesion [41] and the distribution of magnetic and electric domains [42].

2.2.2 Speed limitations of AM-AFM

Similar to the analysis of CM-AFM, the free oscillation of AFM probe can be modeled as [43, 44]

$$m\ddot{z} + c\dot{z} + kz = F_0 \cos\ \omega t \tag{12}$$

where z is vertical position of AFM tip; m, c and k represent the first modal mass, damping constant and stiffness of a lumped cantilever; F_0 is the excitation force that drives the cantilever's oscillation. The general solution of Eq. (12) is

$$z(t) = Ce^{-\omega_n t/2Q} \cos(\omega_n \sqrt{1-\zeta^2} t + \varphi_1 + \frac{F_0/m}{\sqrt{\left(\omega_n^2 - \omega^2\right)^2 + (\omega\omega_n/Q)^2}} \cos(\omega t - \varphi_2) \tag{13}$$

where

$$\varphi_2 = acr\ tan \frac{\omega\omega_n/Q}{\omega_n^2 - \omega^2}, \tag{14}$$

C and ϕ_1 are determined by the initial condition, and the natural resonant frequency $\omega_n = \sqrt{k/m}$.

Equation (13) indicates that the transient process of probe motion exhibits an oscillatory damping behavior, where the time constant is given by $2Q/\omega_n$. As a result, probes with higher resonant frequencies and lower quality factors result in smaller time constants and more transient behavior, as shown in Fig. 3. This implies that the probe can transition faster between states. In high-speed AM-AFM, the rapid transition of the probe between steady states is crucial and directly affects the quality of the resulting images.

Furthermore, to derive the transfer function of cantilever in AM-AFM, T. Sulchek et al. [43] proposed to analyze the scanning process over a downward step, as shown in Fig. 3. The transient amplitude as a function of time is

$$A(t) = -\left(A_f - A_{sp}\right)e^{-\omega_n t/2Q} + A_f, \tag{15}$$

where A_f and A_{sp} are free oscillation amplitude and the setpoint amplitude, respectively. The normalized amplitude increase as a function of time is given by

$$\Delta A(t) = \frac{A_{sp}}{A_f}\left(1 - e^{-\omega_n t/2Q}\right) = \alpha(1 - e^{-\omega_n t/2Q})\ \ (0 < \alpha < 1) \tag{16}$$

where $a = A_{sp}/A_f$. The Laplace transform of Eq. (16) describes the frequency-domain response of the probe's amplitude variation when subjected to a step signal, and thus cantilever's transfer function is

$$G_c(S) = \frac{\alpha\omega_n/2Q}{s + \omega_n/2Q} = \frac{\alpha}{2Q/\omega_n s + 1} \tag{17}$$

Equation (17) shows that the amplitude variation of the probe behaves like a typical first-order inertial system, with -3 dB bandwidth of $\omega_n/2Q$. Therefore, to improve the imaging bandwidth and thus enhance the operating speed, increasing the resonant frequency of the probe while reducing its quality factor are effective solutions.

It is important to recognize that there is an inherent tradeoff in AM-AFM operation associated with the Q factor of the cantilever [46]. High-Q cantilevers are more sensitive to changes in topography, but their long ring-up time requires slower scan speeds. Because of this limitation, AM-AFM is rarely used in vacuum as the Q factor of the sensor is usually so high that the cantilever oscillates many times before the amplitude settles to its new value. On the other hand, low-Q cantilevers are less sensitive to changes in interaction forces, but they react more quickly to changes in topography. In other words, increasing the scanning speed comes at the expense of sacrificing the sensitivity.

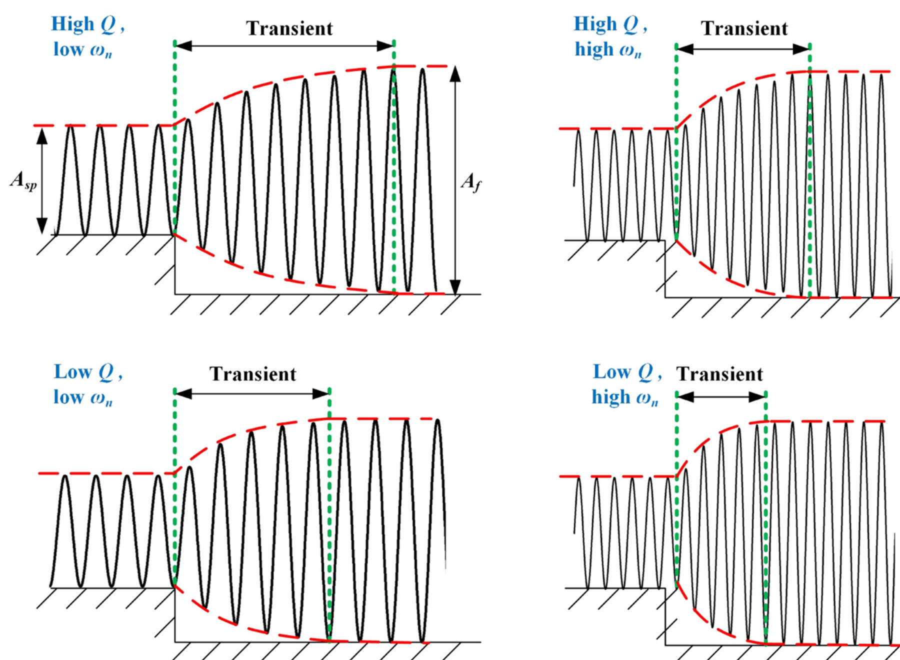

Fig. 3 Tapping mode speed limit analysis using a downward step. Redrawn according to [43] and [45]

2.3 Frequency modulation mode

2.3.1 Operating principle of FM-AFM

Frequency modulation atomic force microscopy (FM-AFM) distinguishes itself from CM-AFM and AM-AFM by achieving truly non-contact measurement of the sample surface. Such an operating mode was originally proposed by Albrecht et al. in 1990, shortly after the invention of AFM [47]. In FM-AFM, rather than maintaining continuous physical contact or intermittent contact with the sample, a small excitation signal is applied to the cantilever, causing it to vibrate near its resonance frequency with a typical amplitude ranging from several nanometers up to less than 10 nm [48]. The tip is positioned close to the sample surface, but without making direct contact. As the tip-sample interaction forces change the frequency of the cantilever's oscillation, these frequency variations are measured and used to generate high-resolution images and gather other information about the surface properties.

The operational principle of FM-AFM, illustrated in Fig. 4, involves three feedback loops [49]. The first is an amplitude control loop, denoted by ④, which measures the amplitude A of the signal and compares it with a setpoint to determine the amplification of the excitation signal ⑥for the cantilever. To measure the frequency of the cantilever, a phased-locked loop (PLL) is employed, which maintains a fixed 90° phase difference between the input and output of the PLL. The outputs of the amplitude control loop and the PLL are then used to synthesize the excitation signal of the shaking piezo to sustain a constant amplitude of the cantilever during operation. The third feedback loop, represented by ⑦, maintains a constant frequency shift by adjusting the distance between the tip and the surface (z position).

The non-contact nature of FM-AFM offers several advantages [50]. Firstly, it minimizes the chance of sample damage, making it particularly suitable for delicate or soft samples. Secondly, FM-AFM allows for the imaging of surfaces that are difficult to access in contact mode, such as samples with liquid layers or soft coatings. Additionally, the absence of direct contact reduces the influence of lateral forces, leading to more reliable measurements.

However, as FM-AFM operates with the aid of three independent control loops, it is inherently more complex than CM-AFM and AM-AFM. Nevertheless, the qPlus sensor, invented by physicist Franz J. Giessibl [51], has emerged as a widely accepted and powerful core for FM-AFM. Originally made from a quartz tuning fork with only one tine oscillating, the qPlus sensor features self-sensing capabilities as the deflection signal is obtained via the piezoelectric effect [9, 52]. Its compact size also makes it especially valuable for high-vacuum environments where the chamber space is limited.

2.3.2 Speed limitations of FM-AFM

According to operating principle discussed in previous subsections, the key difference between AM-AFM and FM-AFM is the use of two additional control loops: the amplitude control loop and the frequency measurement loop. Therefore, the system dynamics of FM-AFM can be built

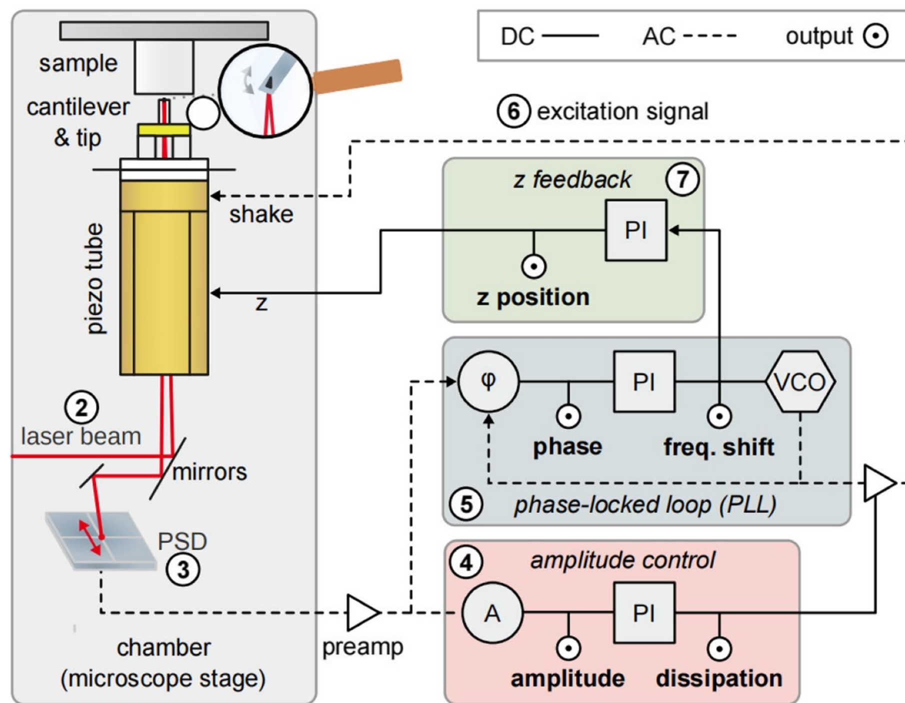

Fig. 4 Schematic of the frequency modulation AFM [49]

on existing results of AM-AFM, with additional considerations for the dynamics of the two extra loops.

Kilpatrick et al. [53] modeled the transfer functions of these two loops as follows:

$$G_A(s) = \frac{A_{cant}(\omega_n)}{A_d(\omega_n)} \frac{1}{s + \frac{\omega_n}{2Q}} G_{lock-in}(s) \tag{18}$$

$$G_\phi(s) = \left(\frac{\partial \phi_{cant}}{\partial \omega_d} | \omega_d = \omega_n \right) \frac{1}{s + \frac{\omega_n}{2Q}} G_{lock-in}(s) \tag{19}$$

where $A_{cant}(\omega)$ and $\Phi_{cant}(\omega)$ represent cantilever's amplitude and phase responses, respectively; $A_d(\omega)$ is the cantilever driving amplitude; $G_{lock-in}(s)$ is the frequency response of the lock-in amplifier; ω_n is the natural resonant frequency of the cantilever. Compared to the system dynamics of AM-AFM, as given by Eq. (17), the unique component in FM-AFM is the PLL or lock-in amplifier. Therefore, achieving high-speed operation in FM-AFM requires improving the bandwidth and latency time, in addition to optimizing other components for high-speed operation of AM-AFM.

3 State-of-the-art HS-AFM solutions

3.1 Enabling techniques of high-speed CM-AFM

In the preceding Sect. 2.1.2, an in-depth investigation was carried out to examine the critical factors that restrict the high-speed operation of CM-AFM, with a specific focus on the tip-sample interactions. Equation (8) and Eq. (10) highlight the significance of a small quality factor and a large resonance frequency in ensuring optimal high-speed performance. Furthermore, it is important to consider the response time of the feedback loop in both the lateral (X–Y) and vertical (Z) directions when addressing CM-AFM. In this section, we will conduct a systematic review of the enabling techniques that facilitate high-speed operation in CM-AFM.

3.1.1 High-frequency cantilevers

The angular resonant frequency ω_0 and the spring constant k_c of a rectangular cantilever with thickness d, width w, and length l are expressed as [54]

$$\omega_0 = 1.02 \frac{d}{l^2} \sqrt{\frac{E}{\rho}} \tag{20}$$

$$k_c = E \frac{wd^3}{4l^3} \tag{21}$$

where E and ρ are Young's modulus and the density of the cantilever, respectively. To enhance the operation speed, one intuitive approach is to increase ω_0 by either reducing the length or increasing the thickness of the cantilever, as suggested in Eq. (20). However, fabricating thicker cantilevers may not be an optimal solution. This

is because the spring constant is directly proportional to the cubic power of the thickness, leading to a significant increase in interaction forces during CM-AFM scanning. Consequently, Hansma's group proposed the development of short silicon nitride cantilevers with varying lengths ranging from 23 to 203 μm [55], while maintaining a thickness in the range of several hundred nanometers (See Fig. 5a) [54, 56]. The small cantilever permitted fast imaging of calcite crystal growth at scan rates of 104 lines/s [57]. Ando's group took a step further by reducing the geometric dimensions of the cantilever to 140 nm thick, 2 μm wide, and 10 μm long [58, 59]. The cantilevers' resonance frequency exceeded 1 MHz, and their spring constants were below 0.3 N/m, greatly exceeding those of typical AFM cantilevers. The authors also developed an extremely long and thin tip by attaching amorphous carbon to the cantilever (Fig. 5b), and thus led to image the surface structure of live cells with a high spatiotemporal resolution [58]. Ivo Rangelow's group developed fast active cantilevers (Fig. 5c) and cantilever array (Fig. 5d), which integrates actuator and sensing elements into the probe [60, 61]. However, it was evaluated that the practical upper limit for the attainable resonant frequency of small cantilevers was no more than 3.5 MHz in water [24]. This limitation occurs because the cantilever supporting base tends to eclipse the incident laser beam used in the optical beam deflection (OBD) detector. In view of this issue, a new type of probe (Fig. 5e) based on cavity optomechanics was recently developed [62–64]. These probes exhibit a remarkable 130 MHz mechanical resonance mode, surpassing the resonant frequencies of existing short probes by two orders of magnitude. Furthermore, the utilization of optomechanical detection has demonstrated outstanding measurement resolutions. The probes have exhibited the capability to achieve sub-picometer amplitudes in vibration, a level of operation that was previously unattainable with current AFM technologies. The authors of [62] foresee that such advancements have the potential to revolutionize next-generation HS-AFM, enabling ultra-high-speed imaging with frame rates reaching milliseconds per frame.

3.1.2 Fast AFM scanner

The AFM scanner moves either the sample or probe in three dimensions, allowing it to track variations in the topography of the sample surface. Therefore, the mechanical bandwidth of the scanner significantly impacts the speed of scanning. Ando et al. presented the first high-bandwidth scanner design in 2001 (Fig. 6a1) [59]. The developed scanner used separate sets of stack PEAs for each of the three scan directions. To minimize the vibrations induced by quick displacements of the Z-actuator, two identical piezo-actuators were mounted in opposite

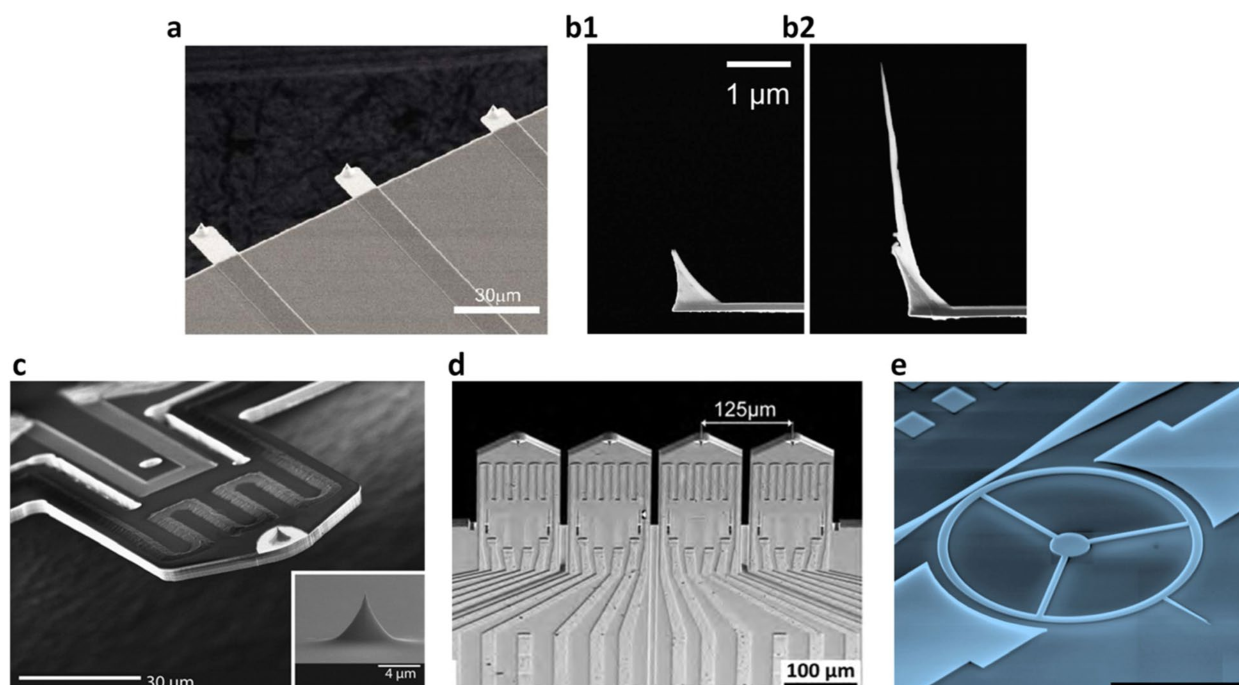

Fig. 5 Representative high-frequency cantilevers for HS-AFM: (**a**) Short cantilevers developed by Hansma's group [56]; (**b**1) and (**b**2) Comparison of regular and long-tip cantilevers developed by Ando's group [58]; (**c**) Active cantilever with integrated actuator and sensing elements [60]; (**d**) Quattro active cantilever array designed by Rangelow's group [61]; and (**e**) Recently proposed optomechanical probe [62]

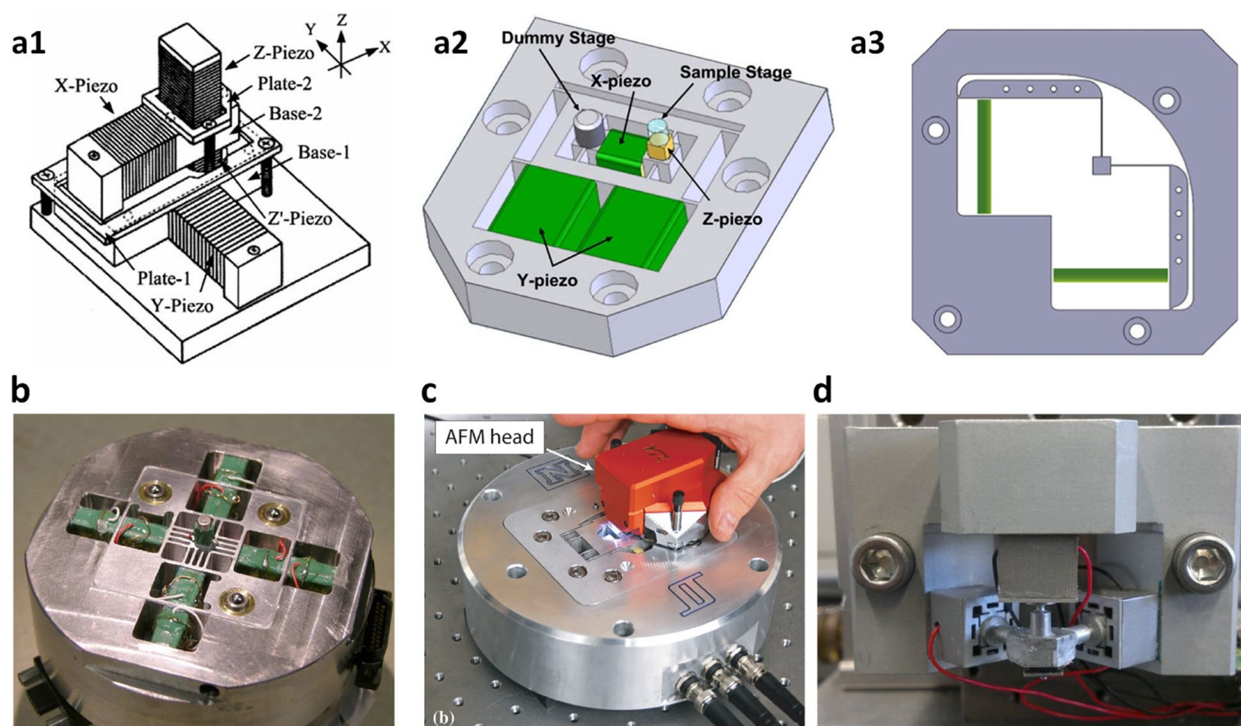

Fig. 6 Fast AFM scanner design: (**a**1)-(**a**3) High-speed AFM scanners developed by Ando's group [22, 59, 67]; (**b**) Scanner with a push–pull configuration developed by Hansma's group [69]; (**c**) Serial-kinematic scanner design [70]; and (**d**) High-bandwidth tripod scanner [71]

directions. The first resonant mode was reported to occur around 60 kHz. Later, an improved design was proposed that utilized mechanical flexures to replace the ball-guide stage in the previous design (Fig. 6a2) [65], and thus is more stable and easier to construct. More recently, an ultra-fast Z-scanner was developed the same group, featuring a resonance frequency above 1.1 MHz [66]. The scanner utilizes a small piezo-stack supported at its bottom four vertices on a cone-shaped hollow, which maintains the resonance frequency of the Z-scanner at the same level as that of the piezo in free vibration. While these designs have extremely high resonance frequencies, one drawback is their limited scan range, which is typically less than 1 μm. To address this issue, a wide-area scanner (Fig. 6a3) was developed that employs a leverage mechanism to magnify the displacements of stack actuators [67, 68], resulting in a maximum XY scan range of 46 × 46 μm^2. Because of a lower resonance frequency of 2 kHz, this design achieves an imaging rate of 3 s per frame.

Fantner et al. introduced another classical high-speed scanner design comprised of multiple piezo-stack actuators and comb-flexures (Fig. 6b). The comb-flexure is an array of vertical blade springs that are rigid in the direction of the piezo's motion and flexible in one of the perpendicular directions. This design achieved a resonance frequency of 23.4 kHz, with a scan range of 15 μm in the X and Y directions and 6 μm in the Z direction. By utilizing this scanner, an imaging rate as high as 8 frames per second was achieved. Kenton et al. also developed a high-bandwidth nanopositioner based on a serial-kinematic design (Fig. 6c), which employs vertically stiff, double-hinged serial flexures to guide the motion of the sample stage [70]. The lateral and vertical ranges of the nanopositioner were 9 μm × 9 μm and 1 μm, respectively, with resonance frequencies of 24.2 kHz, 6 kHz, and 70 kHz. As the mass of the sample stage has a significant impact on the mechanical bandwidth, Yang et al. developed a rigid tripod scanner in which three scanning axes mutually support each other (Fig. 6d), enabling each axis to achieve high resonance frequencies above 20 kHz [71].

Besides flexure-based scanner design, Humphris and co-workers utilized the resonance of a tuning fork to generate fast scanning motions [72]. This allowed constant height CM-AFM imaging of 5 × 5 μm^2 area at approximately 50 fps. Picco et al. improved this design by using a combined tuning fork and flexure-stage scanning system [73]. As no feedback involved in the Z-direction, the scanning speed was only limited by the cantilever dynamics and thus was capable of ultra-high-speed imaging in excess of 1000 fps. Building on a similar concept, Zhao et al. extended the scan range to 37.5 μm and achieved an imaging time of less than 1 s per frame

[74]. As the interaction forces are essentially uncontrollable, it is important to have a sufficiently flat sample surface to minimize their effects.

3.1.3 Wide-bandwidth power drive

Existing HS-AFM scanner were usually actuated by piezoelectric stacks. Electrically, these actuators are nonlinear capacitive loads that demand high voltage and large output current when operating at high frequencies. Meeting these requirements presents a significant challenge in the design of power drives, typically voltage amplifiers. To tackle this problem, Fleming designed a dual amplifier that achieved a small-signal bandwidth of 2 MHz with a 100 nF capacitive load [75]. The dual amplifier comprises of a high-voltage amplifier and a fast low-voltage amplifier, which work in tandem to enhance performance at higher frequencies. However, the developed dual-amplifier arrangement has a worst-case power dissipation of only 30 W, which reduced travel range at high frequencies. Wang et al. carefully analyzed the stability of a piezo drive with an emitter follower, and further proposed a compensation scheme [76]. Xu et al. considered the amplifier circuit as a closed-loop system, and applied classical control theory to tune the parameters. As a result of these efforts, the developed piezo driver was able to achieve a bandwidth of up to 50 kHz, with ripples less than 2 mV [77].

Another fascinating type of power drive for HS-AFM scanners is the charge drive, which seeks to integrate hysteresis and creep control capabilities into the drive circuit. Charge drive utilizes the linear relationship between the inflow charge and the resulting displacement to drive piezo-actuators. The unfavored hysteresis and creep nonlinearities can thus be avoided. Historically, Comstock first pointed out that the relationship between the free charge and the displacement of PEAs is almost linear [78]. A more detailed analysis was provided by Main et al. in [79]. By far, couples of new implementation schemes have been proposed, including resistive dc feedback with an inverse configuration [80], grounded-load [81], diode-based stabilization [82] and active dc stabilization [83], etc. In addition, digital electronics [84] and switched capacitor technique [85] have also been chosen for hardware implementations. Despite being proposed four decades ago, charge drives have not been widely adopted in industry due to the limited quasi-static performance, stroke loss, difficulties in matching ac and dc gains, and long settling times. To address these issues, Yang et al. proposed the concept of nonlinear charge control [86] and further developed a charge drive with decoupled and self-compensating configurations [87]. It was shown in [87] and [88] that hysteresis induced imaging distortions have been well suppressed. A comprehensive review by Yang et al. [89] summarized the latest research developments in this field.

3.1.4 Advanced control strategies

High-speed CM-AFM necessitates advanced control strategies to fulfill two crucial objectives. Firstly, the precision and speed of scanning motion can be adversely affected by piezoelectric hysteresis, creep, and mechanical resonance. The successful mitigation of these issues heavily relies on the implementation of control solutions. Secondly, innovative control strategies are required to accurately regulate the contact force, minimizing its impact on the sample surface and guaranteeing the reliable and robust operation of CM-AFM.

To mitigate the impact of undesired nonlinearities and resonance, feedforward control approaches have gained widespread adoption. The fundamental concept revolves around accurately modeling the system dynamics and subsequently constructing an inversion-based compensator. For instance, numerous hysteresis models have been developed for this purpose, such as the Bouc-Wen model [90], Prandtl-Ishlinskii model [91], polynomial model [92] and others. Based on these models, inverse hysteresis compensators have been designed via the inverse multiplicative structure [93], disturbance-observer-based inversion method [94] and adaptive inverse method [95], just to name a few. The interested reader may refer to review paper such as [96] for details. Similar idea works for creep effect compensation [97]. As for feedfoward vibration control, there are several well-established methods, including optimal inversion [98], notch filter [99] and input shaping techniques [100]. However, the major drawback of feedforward control lies in its inability of dealing model uncertainties and external disturbances. Thus, feedback control strategies have been developed. Given that the scanning path is periodic and highly repetitive, iterative learning control [101] and repetitive control [102] has been considered as a good solution to guarantee precision motion of AFM scanner. By treating undesired nonlinearities and resonance as a lumped disturbance, disturbance rejection based control strategies, such as sliding mode control [103] and disturbance observer based control [104], have been shown to be effective. Additionally, model-based control strategies were also developed to optimize motion control performance based on prior knowledge of the scanner's dynamics. Model predictive control [105], internal model control [106], and H_{inf} control [107] are representative methods falling under this umbrella. The interested readers are recommended to refer to [108] and [109] for further details.

Regarding contact force control, Ren et al. proposed adjusting the cantilever deflection set-point for each scanline to the minimum level necessary for stable

probe-sample contact [110]. To enhance sample topography tracking, they integrated a data-driven iterative feedforward control, which utilizes a prediction of the next-line topography, into the topography feedback loop. Swiadkowski et al. devised active electromagnetic cantilevers to accurately regulate the force applied to the sample [111]. Furthermore, they implemented a predictive proportional-integral-derivative controller to achieve nearly zero interaction force. Likewise, Lavanya et al. suggested regulating the tip-sample force through magnetic actuation, which utilizes real-time topography estimation to cancel out the interaction force [112]. A reduction by a factor of 12 in the variation of interaction force was demonstrated. These efforts have significantly addressed the challenge of high-speed CM-AFM.

3.1.5 Various scanning paths

AFM commonly employs raster or zig-zag paths to scan over the X–Y plane, due to its advantages of a constant scanning velocity together with evenly distributed pixel resolutions. However, the triangular trajectory introduces odd harmonics that can excite the mechanical resonance of the scanner, leading to significant tracking errors. The scanning line rate is thus typically limited to 1% of the scanner's fundamental resonance frequency [113, 114]. In addition, the slow, step-like motion of the slow axis may cause a creep effect that can result in feature drift in the AFM images [115].

To address concerns with the triangular scanning trajectory, various alternative scanning paths have been proposed. The key concept behind these new designs lies in replacing the triangular trajectory with a sinusoidal trajectory. Building upon this idea, Fleming et al. proposed a sinusoidal raster scanning path, where the fast axis of the AFM scanner is driven by a sinusoidal trajectory while the slow axis is actuated in steps [116]. In addition to the sinusoidal raster scanning path, Mahmood proposed a spiral scanning path (Fig. 7a1) that combines sinusoidal and cosine trajectories of the same frequency but different amplitudes [117]. This approach offers benefits such as uniform scanning and a limited frequency spectrum. Lissajous (Fig. 7b1) is another alternative non-raster scanning pattern that can achieve high-speed imaging, which tracks a purely sinusoidal signal with fixed amplitude but varying phase and frequency [118]. Yong et al. presented the cycloid scan pattern (Fig. 7c1), involving a sinusoidal trajectory in one axis and a combination of sinusoidal trajectory and a ramp input in the other axis [119]. This pattern enables video-rate imaging even though the scanner has a relatively low mechanical bandwidth [120]. Ziegler et al. also proposed an optimized spiral scanning path that combines a constant angular velocity spiral in the center and transitions to constant linear velocity toward the periphery. This approach achieves a high-speed imaging rate of multiple frames per second while maintaining high data density and distribution [121].

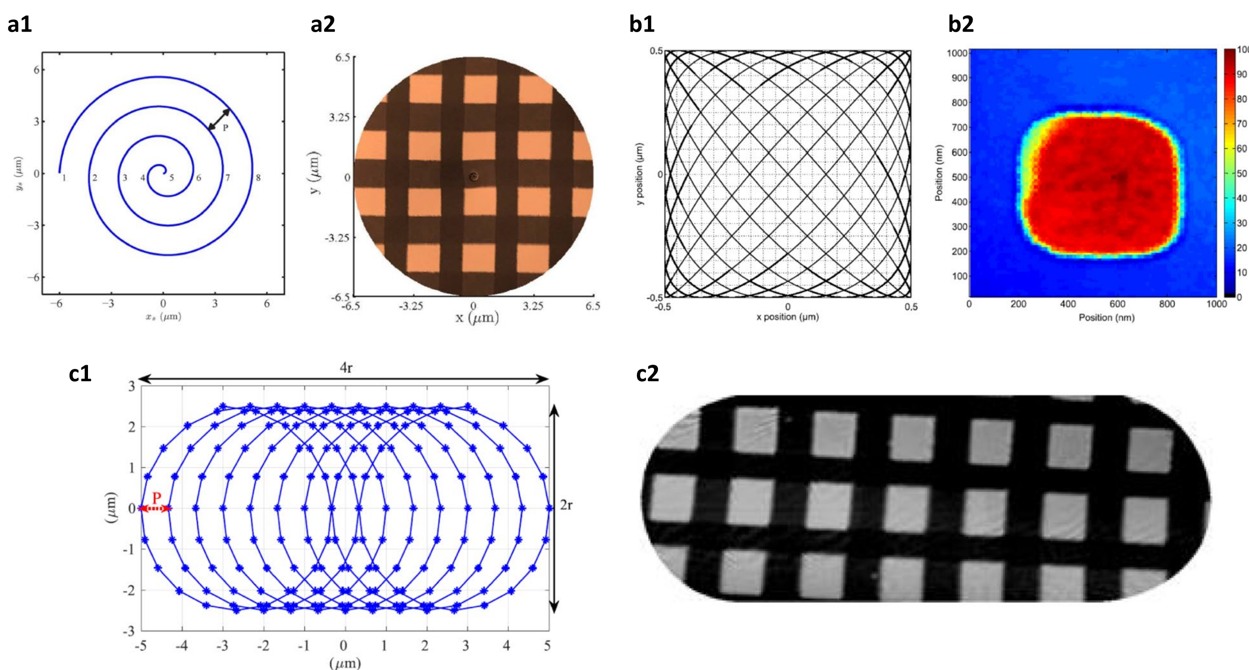

Fig. 7 Representative scanning paths for high-speed scanning: (**a**1) Spiral path [117]; (**b**1) Lissajous path [118]; (**c**1) Cycloid path [119]. (**a**2), (**b**2) and (**c**2) are corresponding imaging results

3.2 Enabling techniques of high-speed AM-AFM

The key distinction between CM-AFM and AM-AFM lies in that the cantilever vibrates around its resonance frequency in AM-AFM. Section 2.2.2 highlight the crucial role of the cantilever's natural resonance frequency and Q-factor in achieving high-speed AM-AFM. Building on the progress described in the previous section regarding the fabrication of small cantilevers, this section will start from the regulation methods for controlling the Q-factor.

3.2.1 Q-control of cantilever

The Q-factor of a cantilever can be regulated using two primary approaches: passive damping, achieved by changing the material properties, and active damping, implemented through design control strategies.

Passive damping involves selecting cantilever materials with high damping coefficient. Towards this end, Adams et al. proposed to use cantilevers made of viscoelastic material to mimic the high damping environment in fluid, yielding cantilevers with inherently low quality factors in any medium [45]. The fabricated polymer cantilevers exhibited a 19 times improvement of detection bandwidth when imaging in the air. In [122], researchers successfully fabricated hydrogel cantilevers with intentionally low Q-factors. The utilization of hydrogel materials in the fabrication process not only enabled enhanced imaging capabilities but also facilitated a simpler, faster, and more affordable manufacturing route for HS-AFM instrumentation.

Active damping, on the other hand, focuses on implementing feedback control to regulate the Q-factor. Sulcheck et al. proposed to use the on-chip actuator to add a force that is proportional to the velocity of the cantilever for frequencies in the imaging bandwidth [46]. As a result, the Q-factor was successfully reduced by a factor of 20. Coskun developed a positive position feedback controller to actively tailor the Q-factor of the cantilever [123]. The effect of Q control on the cantilever's transient response has been illustrated via fast AFM imaging. Likewise, another promising approach for Q-factor regulation is piezoelectric shunt control, which utilizes an electrical impedance placed in series with the tip oscillation circuit to regulate the mechanical damping [124].

3.2.2 Fast amplitude estimation

In AM-AFM, accurately estimating the surface topography requires precise regulation of a cantilever's vibrating amplitude. A rms to dc converter is typically employed, which comprises a rectifier circuit and a low-pass filter [22]. However, inaccurate amplitude estimates can arise if there are additional frequency components in the displacement signal. In such cases, high-frequency oscillations must be removed from the low-bandwidth amplitude estimate, resulting in long convergence times which limits the imaging bandwidth in AM-AFM.

In response to this challenge, Ando et al. devised a peak-hold solution specifically designed for high-speed AM-AFM [59]. This novel technique entails capturing the maximum and minimum voltages of the cantilever oscillation and calculating the difference as the amplitude. By utilizing this approach, video-rate topography imaging in liquid environments becomes attainable [125]. It should be noted that a drawback of this technique is its susceptibility to noise interference. Another effective approach for amplitude estimation is the well-known Lock-in amplifier (LIA). Nonetheless, its primary limitation stems from the utilization of a low-pass filter to eliminate high-frequency components during the mixing process [126]. To overcome this limitation, Karvinen et al. developed a high-bandwidth LIA that incorporates phase cancellation to precisely eliminate the 2ω component, resulting in a significantly broader low-pass filter bandwidth [127]. Additionally, Ragazzon et al. devised a strictly positive real Lyapunov design approach to achieve the same objective, which led to the development of a high-bandwidth Lyapunov estimator with low complexity [128]. The enhanced imaging capabilities of AM-AFM further validated the effectiveness of the developed techniques.

3.3 Enabling techniques of high-speed FM-AFM

FM-AFM can be viewed as a natural evolution of AM-AFM. Consequently, the enabling techniques mentioned in AM-AFM, such as small cantilevers and Q-control techniques, continue to hold importance in FM-AFM as they contribute to the overall performance of the system.

On the other hand, the distinguishing factor in FM-AFM lies in the incorporation of the phase-locked loop (PLL) circuit. PLL plays a crucial role in FM-AFM by serving dual purposes: detecting vibration frequency and generating a cantilever excitation signal based on the cantilever deflection. In a conventional PLL setup, a low-pass filter is employed to generate a phase signal (Fig. 8a). However, the use of this filter introduces a significant latency, consequently limiting the overall bandwidth [129]. Recognizing these issues, Fukuma et al. put forward a novel PLL circuit to enhance the bandwidth and thus reduce the latency (Fig. 8b) [130, 131]. In this arrangement, a phase detector utilizing a high-pass filter is positioned outside of the phase feedback loop. By detecting the phase difference between the deflection and excitation signals through a subtraction circuit with minimal latency, such a PLL circuit achieves more than 10 times improvement in terms of detection bandwidth, thus enables atomic-resolution imaging in liquid at a rate of 1 frame per second [130]. This remarkable achievement has established high-speed atomic-resolution imaging as a

(a) Conventional PLL with low-pass filter

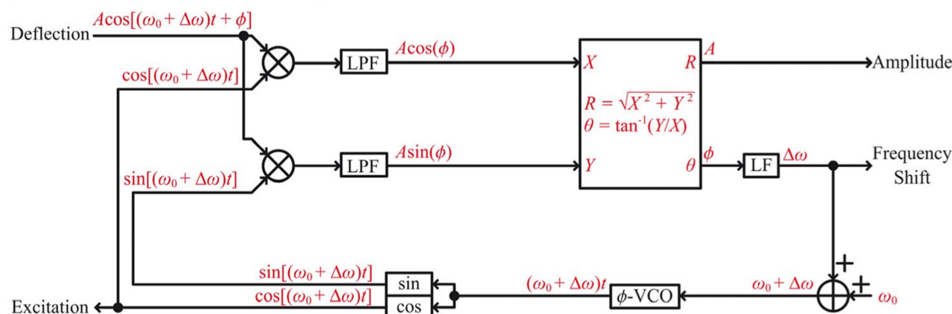

(b) Subtraction-based PLL with high-pass filter

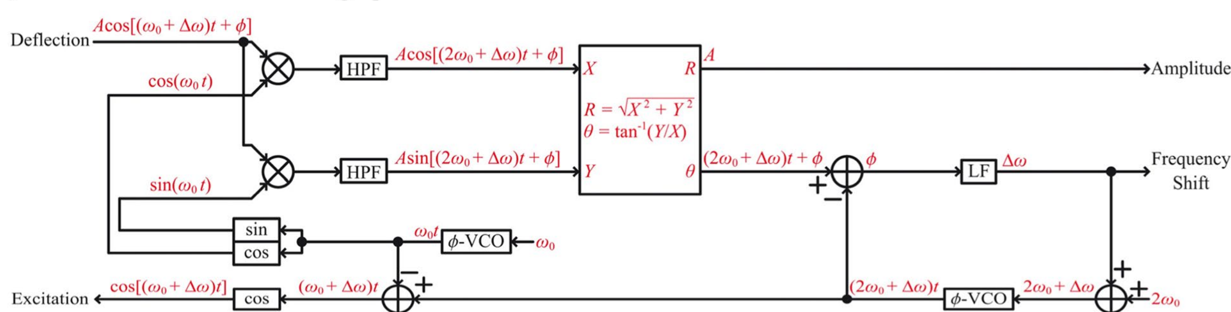

Fig. 8 Schematics of (**a**) conventional PLL with low-pass filter and (**b**) low-latency subtraction-based PLL [130]

routine practice, enabling successful investigations of various dynamic processes, such as calcite dissolution [132] and Chitin Nanocrystal–Water Interfaces [133].

4 Applications in nanofabrication and metrology

4.1 High-throughput tip-based lithography (TBL)

Tip-based lithography has emerged as a promising alternative to conventional lithography for creating structures with nanoscale features. A variety of techniques have been developed to modify materials at the interface between the probe and surface, resulting in different lithography methods. By using a sharp tip in contact or close proximity to a nanoscale area of a sample surface, it becomes possible to control a wide range of processes, including mechanical, thermal, electrostatic, chemical interactions, or various combinations thereof.

While TBL holds great potential for creating nanostructures, the limited throughput has hindered its practical applications. Nevertheless, recent developments of HS-AFM technology have significantly mitigated this gap, rendering TBL an increasingly attractive form of nanolithography for industrial applications. Historically, Quate and co-workers pioneered this field by patterning 40 nm features in siloxane, with writing speeds in excess of 1 mm/s [134]. Szoszkiewicz et al. [135] developed a technique utilizing a resistively heated AFM cantilever (Fig. 9a) to locally heat a thin film of p(THP-MA) on glass to 140 °C, resulting in the creation of controlled chemical patterns with high density and resolution. This technique was shown to write and read chemical patterns at speeds faster than 1 mm/s, with a sub-15 nm feature size and a line density of 2×10^7 lines/m. Miles' group performed local oxidation (Fig. 9b) by applying a voltage between the tip and sample to fabricate silicon oxide nanostructures on a silicon surface [136]. They were able to fabricate oxide features during imaging, with relative tip-sample velocities of up to 10 cm/s and a data capture rate of 15 fps. Besides, Dip-pen nanodisplacement lithography (DNL) is another powerful technique for fabricating 3D polymer nanostructures. Chen et al. [137] conducted a systematic investigation of the molecular displacement mechanism of dip-pen nanolithography (DNL), leading to ultrafine control of 3D structures and high-speed patterning simultaneously. The study demonstrated a significant enhancement of the fabrication speed by up to 200-fold. More recently, Yao et al. [138] reported a high-speed surfing probe technique to continuously pattern the substrate surface at a linear velocity of meters per second (Fig. 9c). The fast scan motion of the writing probe is precisely controlled by using self-adaptive hydro- and aerodynamics functions of a patterning head. The direct writings of nanoscale patterns were

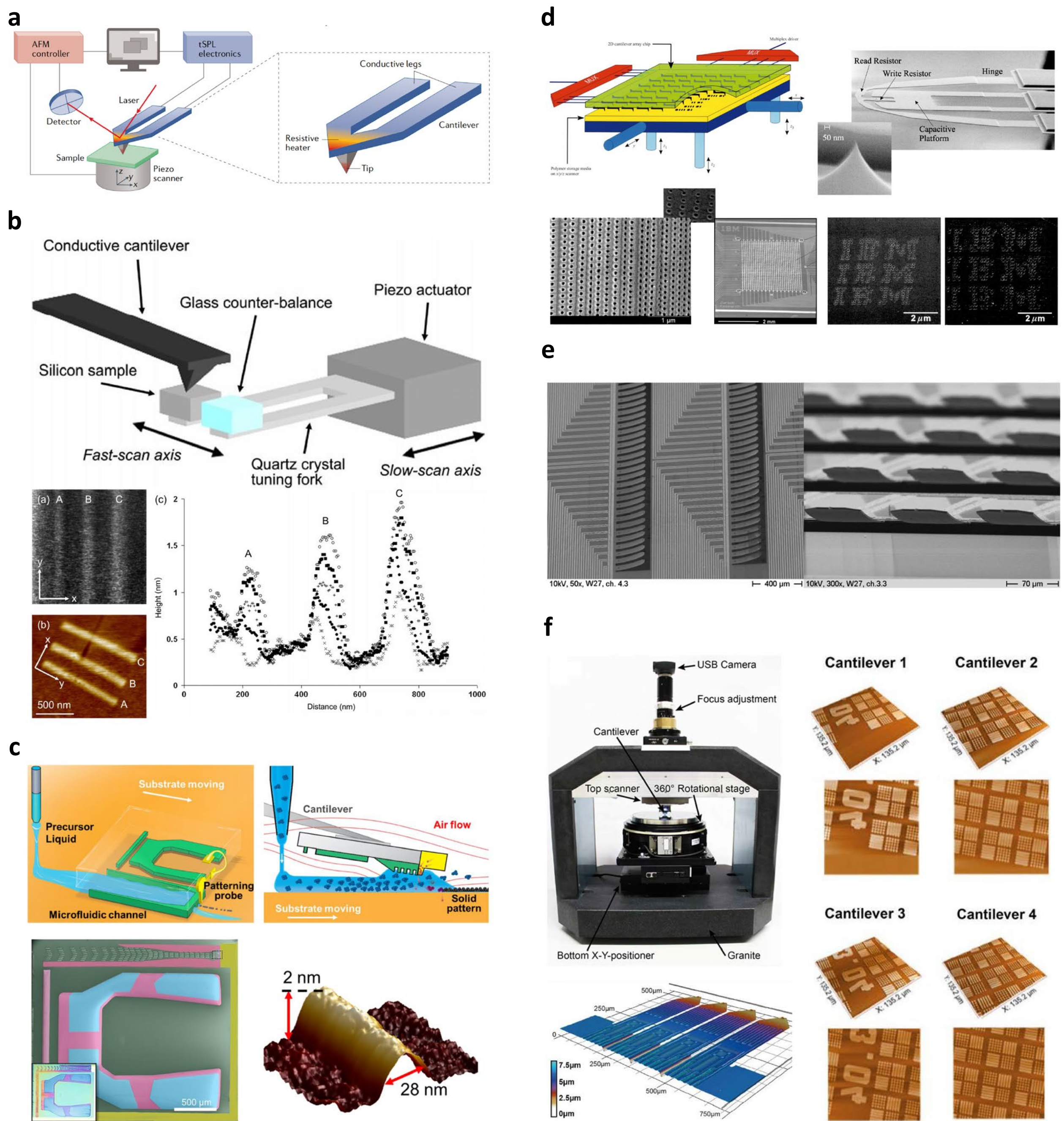

Fig. 9 High throughput tip-based lithography (TBL) enabled by HS-AFM. **a** Components of typical thermal TBL set up [17]. **b** Real-time local oxidation via a customized HS-AFM [136]. **c** High-speed surfing probe lithography achieving a pattern rate of meters per second [138]. **d** "Millipede" project with more than 1000 tips for data storage [139]. **e** Parallel self-sensing and self-actuated proximal probes for electrostatic lithography [140]. **f** AFM system capable of field-emission scanning probe lithography on 150 mm wafers [141]

achieved by ultrafast electron-induced deposition inside a nanoscale flow at a patterning frequency of 20 MHz.

Considering that TBL is essentially a serial process, another straightforward solution to enhance the throughput is by developing parallel TBLs. The early work in this field was conducted by Quate's group, which utilized an array of 50 cantilevers operating in parallel for simultaneous imaging and local oxidation over areas as large as 100 mm^2 [142]. This approach achieved tip speeds of 1 mm/s for imaging and 1 μm/s for lithography. IBM

expanded on this multiple-probe concept by developing a data storage system named Millipede (Fig. 9d) [143]. Millipede utilized a large array of AFM-type cantilevered tips (64 × 64) to write, read, and erase data on very thin polymer films, resulting in a storage density exceeding 1 Tbit/in^2. Rangelow's group developed a massively parallel cantilever platform, consisting of 128 self-sensing and self-actuated proximal probes (Fig. 9e) for electrostatic lithography. Furthermore, the authors developed an AFM system capable of field-emission scanning probe lithography on 150 mm wafers (Fig. 9f), providing excellent stitching accuracy of better than 3 nm [141]. Although still in the early stages, this system may pave the way for reliable single digit nanometer lithography in the near future [144].

4.2 High-speed surface metrology at the nanoscale

HS-AFM technique has gained significant attention as a promising solution for meeting the demands of high-speed nanoscale metrology. Dai et al. from the National Metrology Institute of Germany have made notable advancements in developing a high-speed metrological large range AFM (Fig. 10a) [145]. Their experimental investigations have demonstrated remarkable performance, achieving step height measurements with an accuracy below ± 0.7 nm, together with a high scan speed up to 1 mm/s. Based on these achievements, the authors further combined different stages and sensors to cover a wide spatial spectrum of the surface, and realized a new concept of reference areal surface metrology approach [146]. Likewise, Klapetek et al. developed large area high-speed metrology AFM system, which combined an interferometer based large area XYZ positioning stage with a high-speed AFM XY scanner (Fig. 10b), achieved nanometer resolution over a millimeter scan range [147]. In a more recent work, Heaps et al. brings real-time traceability to HS-AFM [148]. In the developed metrological system, the traceable metrology was achieved by using optical interferometry, resulting in traceability for both short-range video-rate images and large-area images obtained from a hybrid long-range positioning system. The high-speed capability together with the higher lateral resolution shows clear advantage in comparison to optical techniques. Furthermore, Zhang et al. introduced a novel approach that combines AFM with microlens-based scanning optical microscopy [149]. This method involves attaching a microlens to the end of the AFM cantilever, with a deposited tip on the sample-facing side of the lens. By incorporating the microlens, the imaging throughput was enhanced by approximately eight-fold compared to a commercial AFM.

Recently, an impressive development has emerged in the field of metrological AFM with a novel idea of designing cantilever-free parallel AFMs. This idea might pave the way for further improvements of metrology throughput. Specifically, Cao et al. devised such a novel massively parallel AFM through the combination of a cantilever-free probe architecture and a scalable optical method for detecting probe–sample contact (Fig. 10c) [150]. In their initial demonstration, they employed 1088 probes in parallel, enabling the imaging of a 5 mm wide surface with nanoscale resolution. This new imaging approach has opened new avenues for rapid and high-resolution measurement of surface topography. Likewise, Kim et al. have presented a cantilever-free elastomeric probe design and hierarchical measurement architecture that enables the readily reconstruction of high-resolution and high-throughput topography images (Fig. 10d) [151]. In a single scan, they achieved the acquisition of 100 images over a 1 mm^2 area in less than 10 min using a 100-tip array, which demonstrates the great potential of their approach for large-scale tip integration and its superiority over existing methods.

It is worth noting that tip wear is another critical issue for metrological HS-AFM. Strahlendorff et al. conducted.

a rigorous quantitative investigation on this issue and revealed that high scan speeds, reaching up to 1 mm/s, have minimal impact on tip wear, but they do pose an increased risk of tip breakage [152]. Notably, the study attributed tip wear primarily to the integrated dissipated energy, while tip breakage was mainly associated with the temporally peak lateral force. Based on these insightful findings, the authors thus envision that the ultimate solution to solve the problem lies in the development of AFM probes capable of true 3D detection of tip-sample interaction forces.

4.3 Nanofabrication process inspection

In ultra-precision fabrication processes, ensuring optimal products highly depend on effective quality control and defect monitoring. As features become smaller and more complex, maintaining high-quality standards and conducting yield analysis become increasingly critical. To achieve this, implementing reliable metrology and inspection techniques in nanofabrication processes is vital for detecting errors and minimizing waste before proceeding to subsequent processing steps. In these application scenarios, HS-AFM stands out from its electron-beam and optical inspection counterparts, due to its seamless integration capability with machining tools. Such an advantage enables in situ and online inspection of various manufacturing processes. Paul et al. [153] from IBM devised a 3D thermal lithography system that offers rapid turnaround by integrating fast thermomechanical writing of a polymer resist with in situ thermoelectric topography sensing. The developed

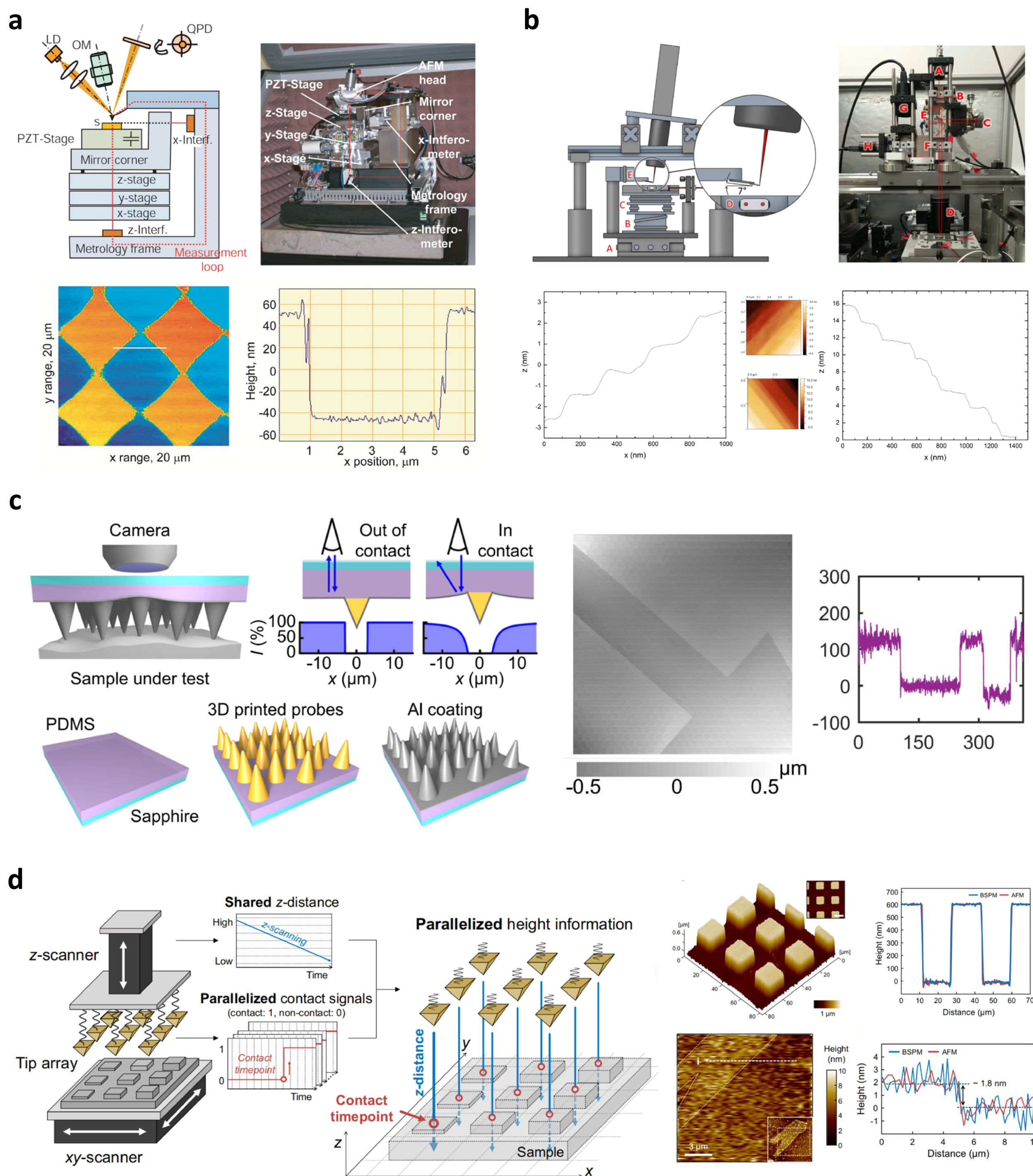

Fig. 10 High-throughput metrology at the nanoscale. **a** High-speed metrological large range AFM developed by National Metrology Institute of Germany, with a scan speed up to 1 mm per second [145]. **b** Traceable metrology AFM with video-rate scan rate [148]. **c** Massively parallel design of cantilever-free AFM probe and applications in nano-metrology [150]. **d** Binary-state AFM with a hierarchical measurement architecture for high-throughput topology measurement [151]

setup permits nanoscale lithography and inspection to be conducted consecutively without the need to remove the sample for a separate development step. The authors demonstrated a linear scan speed of 20 mm/s, a positioning accuracy of 10 nm, and a read-back frequency bandwidth of 100,000 line-pairs/s. Yang et al. designed a

novel tip-scanning HS-AFM and successfully integrated it with focused electron-beam induced deposition process (Fig. 11a) [154]. Such an integration enables in situ measurement of multi-step 3D nano-printing process, showcasing how a complex miniature Swiss mountain Matterhorn has been constructed step-by-step. Furthermore, the developed HS-AFM makes it possible, for the first time, to investigate the evolving mechanical stability immediately after fabrication, and opens a door for various studies such as the morphological change with time in the low nanometer range. Likewise, Rangelow's group has made significant strides by developing a six-axis AFM and integrating it with a high-resolution SEM/FIB system (Fig. 11b) [155]. This combination of AFM, SEM, and FIB technologies presents a plethora of opportunities for hybrid imaging [156], fabrication [157], and analysis [158] of nanostructures. Fantner's group designed a versatile AFM and installed it into the SEM chamber, and thus enabled the inspection of nanoindentation process in vacuum [159]. An updated version of this AFM was then integrated with a helium ion microscope (HIM) (Fig. 11c). This novel instrument achieved in situ correlative analysis and machining at the nanoscale [160]. In addition, Iwata et al. introduced a human-in-the-loop nanomanipulation system that combines a HS-AFM with a haptic device to enable real-time teleoperated nanocutting and nanoindentation tasks. This innovative system bridges the gap between human operators and nanoscale objects, allowing for precise and intuitive manipulation of nanomaterials [161].

The inspection of semiconductor manufacturing processes is a particularly compelling application for HS-AFM. Kohli et al. reported a customized HS-AFM with a height contrast mechanism to obtain wafer surface images, which provides topographic information such as step height, polishing depth and surface roughness [163]. Yao et al. developed a metrology system with an ultimate objective of enabling reliable in-line wafer inspection and quality control [162]. The system is composed of a single-chip AFM, a flexure-based positioning stage, and a passive wafer alignment stage (Fig. 11d). Impressively, the system can complete the entire wafer inspection process in less than a minute, from wafer in to wafer out. The authors then conducted simultaneous, non-contact inspections at multiple hotspots and achieved a throughput of 60 wafers per hour for five-site measurements on a 4-inch wafer [164]. This corresponds to a nanometrology throughput of 66,000 μm^2 per hour. A major concern in HS-AFM inspection lies in its impact on the wafer surface. In their work, Sadeghian et al. conducted a critical evaluation of the issue of surface damage induced by HS-AFM imaging [165]. In particular, the issues of surface damage in four major scanning modes, namely CM-AFM, AM-AFM, FM-AFM, and peak force tapping, are examined to determine the most appropriate modes for various applications. The study revealed that an improper choice of scanning modes and parameters can result in substantial contact stress, which was identified as the primary cause of surface damage. Kohli et al. also conducted a thorough safety factor analysis of the high-speed imaging process and found that applying a force larger than 10 nN to the wafer surface resulted in damage to the pattern [163]. These findings offer AFM users valuable insights into scanning parameters to avoid sample damage during inspection.

5 Future outlook

We have systematically summarized research progress in the past three decades that enable high-speed operation of CM-AFM, AM-AFM and FM-AFM modes. It was shown that Q-factor and natural resonance frequency of the cantilever are essential in governing tip-sample interactions and thus should be optimized for enhancing the operational speed. Regarding the scanning unit, enabling key techniques such as fast scanner design, wide bandwidth power drive, advanced control strategies and novel scanning paths enhance the imaging rate of CM-AFM up to video rate. These shared technologies also serve as the fundamental basis for both AM-AFM and FM-AFM. Furthermore, the Q-control of the vibrating cantilever, along with fast amplitude estimation required by AM-AFM, and the high-bandwidth PLL required by FM-AFM, contribute to high-speed operation of these two modes in liquid environments. The unprecedented operational speed provided by HS-AFM enables high throughput TBL together with in-line metrology and inspection of various nanofabrication processes. In particular, the development of massively parallel AFMs holds tremendous potential for future industrial applications.

Looking ahead, it is crucial to carefully address several open issues, which constitute the future directions in the field of HS-AFM. Firstly, high speed operational modes with gentle applied force such as AM-AFM and FM-AFM, are currently limited to operations in aqueous environments. However, since the majority of nanofabrication processes occur in either ambient or vacuum conditions, there is a strong need for further advancements in Q-factor control through materials design and control strategy development. Tackling this problem will elevate the metrology and inspection capabilities of HS-AFM to an entirely new level. Secondly, to fulfill the essence of nanofabrication, which involves manufacturing large quantities of nanoscale structures at potentially low cost, HS-AFM must possess both high speed and a large scanning range, extending up to at least the millimeter level. This requirement differentiates the developed

Fig. 11 Nanofabrication process inspection with HS-AFM. **a** In situ and online inspection of multi-layer 3D nanoprinting process [154]. **b** In situ inspection of various nanofabrication processes including lithography and nanomachining [156, 158]. **c** Integrated AFM and helium ion beam for in situ nanomachining and analysis [160]. **d** Instrumentation development and measurement results for in-line inspection of nanoscale features in semiconductor manufacturing system [162]

instruments from those primarily used for biological investigations. However, since the scanning range and speed are inherently contradictory in existing designs, there is a strong demand for innovative solutions in the scanning mechanism. Thirdly, while parallel AFMs have shown promising potential, their development is still in the early stages. Contact modes are commonly used for high-throughput inspection and metrology due to their simple configuration. However, this simplicity comes at the cost of tip wear and potential surface damage. On the other hand, AM-AFM and FM-AFM require more complex control electronics for implementation. The scaling up of these techniques for parallel operations remains an open question. Resolving these challenges necessitates persistent and dedicated efforts. Nevertheless, these endeavors hold the promise of propelling HS-AFM beyond the confines of the laboratory, leading to its widespread implementation in real-world applications.

Authors' contributions

Conceptualization: Chen Yang and Wu-le Zhu; Writing and editing: Chen Yang and Chao-qun Dang; Supervision and review: Bing-Feng Ju and Chao-qun Dang.

Declarations

Competing interests

Bingfeng Ju is a member of the editorial board of this journal. He was not involved in the editorial review or the decision to publish this article. All authors declare that there are no competing interests.

Received: 10 August 2023 Revised: 16 August 2023 Accepted: 17 August 2023
Published online: 27 September 2023

References

1. Binnig G, Quate CF, Gerber C (1986) Atomic force microscope. Phys Rev Lett 56(9):930–933
2. Crouzier L et al (2019) Development of a new hybrid approach combining AFM and SEM for the nanoparticle dimensional metrology. Beilstein J Nanotechnol 10:1523–1536
3. Zhou L et al (2017) Progress in the Correlative Atomic Force Microscopy and Optical Microscopy. Sensors (Basel) 17(4):938
4. Surman SB et al (1996) Comparison of microscope techniques for the examination of biofilms. J Microbiol Methods 25(1):57–70
5. Bisterov I et al (2022) On-machine measurement with an electrochemical jet machine tool. Int J Mach Tools Manuf 174:103859
6. Giessibl FJ (2003) Advances in atomic force microscopy. Rev Mod Phys 75(3):949–983
7. Gan Y (2009) Atomic and subnanometer resolution in ambient conditions by atomic force microscopy. Surf Sci Rep 64(3):99–121
8. Fukuma T, Garcia R (2018) Atomic- and Molecular-Resolution Mapping of Solid-Liquid Interfaces by 3D Atomic Force Microscopy. ACS Nano 12(12):11785–11797
9. Giessibl FJ (2019) The qPlus sensor, a powerful core for the atomic force microscope. Rev Sci Instrum 90(1):011101
10. Tseng AA (2011) Advancements and challenges in development of atomic force microscopy for nanofabrication. Nano Today 6(5):493–509
11. Li Z et al (2023) Nanomachining of van der Waals nanowires: Process and deformation mechanism. Int J Mach Tools and Manuf 188:104018
12. Garcia R, Knoll AW, Riedo E (2014) Advanced scanning probe lithography. Nat Nanotechnol 9(8):577–587
13. Ryu YK, Garcia R (2017) Advanced oxidation scanning probe lithography. Nanotechnology 28(14):142003
14. Holz M et al (2019) Tip-based electron beam induced deposition using active cantilevers. J Vac Sci Technol B Nanotechnol Microelectron: Materials, Processing, Measurement, and Phenomena 37(6):061812
15. Fang F et al (2022) Nanometric cutting: Mechanisms, practices and future perspectives. Int J Mach Tools and Manuf 178:103905
16. Wang J et al (2021) Towards understanding the machining mechanism of the atomic force microscopy tip-based nanomilling process. Int J Mach Tools Manuf 162:103701
17. Albisetti E et al (2022) Thermal scanning probe lithography. Nat Rev Methods Primers 2(1):32
18. Howell ST et al (2020) Thermal scanning probe lithography-a review. Microsyst Nanoeng 6:21
19. Minne SC et al (1998) Automated parallel high-speed atomic force microscopy. Appl Phys Lett 72(18):2340–2342
20. Brown BP et al (2013) Opportunities in high-speed atomic force microscopy. Small 9(19):3201–3211
21. Heath GR, Scheuring S (2018) High-speed AFM height spectroscopy reveals micros-dynamics of unlabeled biomolecules. Nat Commun 9(1):4983
22. Ando T, Uchihashi T, Fukuma T (2008) High-speed atomic force microscopy for nano-visualization of dynamic biomolecular processes. Prog Surf Sci 83(7–9):337–437
23. Ando T, Uchihashi T, Kodera N (2013) High-speed AFM and applications to biomolecular systems. Annu Rev Biophys 42:393–414
24. Ando T (2018) High-speed atomic force microscopy and its future prospects. Biophys Rev 10(2):285–292
25. Barrett RC, Quate CF (1991) High-speed, large-scale imaging with the atomic force microscope. J Vac Sci Technol B 9(2):302–306
26. Dufrene YF et al (2017) Imaging modes of atomic force microscopy for application in molecular and cell biology. Nat Nanotechnol 12(4):295–307
27. Müller DJ et al (2020) Atomic Force Microscopy-Based Force Spectroscopy and Multiparametric Imaging of Biomolecular and Cellular Systems. Chem Rev 121(19):11701–11725
28. Santos S et al (2017) Multifrequency AFM: from origins to convergence. Nanoscale 9(16):5038–5043
29. Meyer G, Amer NM (1990) Simultaneous measurement of lateral and normal forces with an optical-beam-deflection atomic force microscope. Appl Phys Lett 57(20):2089–2091
30. Adams JD et al (2005) Self-sensing tapping mode atomic force microscopy. Sens Actuators, A 121(1):262–266
31. Dukic M, Adams JD, Fantner GE (2015) Piezoresistive AFM cantilevers surpassing standard optical beam deflection in low noise topography imaging. Sci Rep 5:16393
32. Jalili N, Laxminarayana K (2004) A review of atomic force microscopy imaging systems: application to molecular metrology and biological sciences. Mechatronics 14(8):907–945
33. Xie H, Haliyo DS, Regnier S (2009) A versatile atomic force microscope for three-dimensional nanomanipulation and nanoassembly. Nanotechnology 20(21):215301
34. Yan Y et al (2010) Top-down nanomechanical machining of three-dimensional nanostructures by atomic force microscopy. Small 6(6):724–728
35. Burns DJ (2010) A system dynamics approach to user independence in high speed atomic force microscopy, in Massachusetts Institute of Technology
36. Butt HJ et al (1993) Scan speed limit in atomic force microscopy. J Microsc 169(1):75–84
37. Hansma PK et al (1994) Tapping mode atomic force microscopy in liquids. Appl Phys Lett 64(13):1738–1740
38. Putman CAJ et al (1994) Tapping mode atomic force microscopy in liquid. Appl Phys Lett 64(18):2454–2456
39. Tamayo J, García R (1997) Effects of elastic and inelastic interactions on phase contrast images in tapping-mode scanning force microscopy. Appl Phys Lett 71(16):2394–2396
40. Bar G, Brandsch R, Whangbo M-H (1998) Effect of Viscoelastic Properties of Polymers on the Phase Shift in Tapping Mode Atomic Force Microscopy. Langmuir 14(26):7343–7347

41. Vlassov S et al (2018) Adhesion and Mechanical Properties of PDMS-Based Materials Probed with AFM: A Review. Rev Adv Mater Sci 56(1):62–78
42. Campbell MP et al (2016) Hall effect in charged conducting ferroelectric domain walls. Nat Commun 7:13764
43. Sulchek T et al (2002) Characterization and optimization of scan speed for tapping-mode atomic force microscopy. Rev Sci Instrum 73(8):2928–2936
44. Mertz J, Marti O, Mlynek J (1993) Regulation of a microcantilever response by force feedback. Appl Phys Lett 62(19):2344–2346
45. Adams JD et al (2016) Harnessing the damping properties of materials for high-speed atomic force microscopy. Nat Nanotechnol 11(2):147–151
46. Sulchek T et al (2000) High-speed tapping mode imaging with active Q control for atomic force microscopy. Appl Phys Lett 76(11):1473–1475
47. Albrecht TR et al (1991) Frequency modulation detection using high-Q cantilevers for enhanced force microscope sensitivity. J Appl Phys 69(2):668–673
48. Giessibl FJ, Bielefeldt H (2000) Physical interpretation of frequency-modulation atomic force microscopy. Phys Rev B 61(15):9968–9971
49. Kling, F.H., Diffusion and structure formation of molecules on Calcite(104). 2018, Johannes Gutenberg-Universität Mainz
50. Fukuma T et al (2005) True atomic resolution in liquid by frequency-modulation atomic force microscopy. Appl Phys Lett 87(3):034101
51. Giessibl FJ (1998) High-speed force sensor for force microscopy and profilometry utilizing a quartz tuning fork. Appl Phys Lett 73(26):3956–3958
52. Huber F, Giessibl FJ (2017) Low noise current preamplifier for qPlus sensor deflection signal detection in atomic force microscopy at room and low temperatures. Rev Sci Instrum 88(7):073702
53. Kilpatrick JI et al (2009) Frequency modulation atomic force microscopy in ambient environments utilizing robust feedback tuning. Rev Sci Instrum 80(2):023701
54. Walters DA et al (1996) Short cantilevers for atomic force microscopy. Rev Sci Instrum 67(10):3583–3590
55. Hansma PK et al (2006) Applied physics. High-speed atomic force microscopy. Science 314(5799):601–602
56. Fantner GE et al (2006) Components for high speed atomic force microscopy. Ultramicroscopy 106(8–9):881–887
57. Paloczi GT et al (1998) Rapid imaging of calcite crystal growth using atomic force microscopy with small cantilevers. Appl Phys Lett 73(12):1658–1660
58. Shibata M et al (2015) Long-tip high-speed atomic force microscopy for nanometer-scale imaging in live cells. Sci Rep 5:8724
59. Ando T et al (2001) A high-speed atomic force microscope for studying biological macromolecules. Proc Natl Acad Sci U S A 98(22):12468–12472
60. Michels T et al (2012) Micromachined self-actuated piezoresistive cantilever for high speed SPM. Microelectron Eng 97:265–268
61. Ahmad A, et al (2016) Large area fast-AFM scanning with active "Quattro" cantilever arrays. J Vac Sci Technol B Nanotechnol Microelectrons: Materials, Processing, Measurement, and Phenomena 34(6)
62. Schwab L et al (2022) Very-high-frequency probes for atomic force microscopy with silicon optomechanics. Microsyst Nanoeng 8:32
63. Doolin C et al (2014) Multidimensional optomechanical cantilevers for high-frequency force sensing. New J Phys 16(3):035001
64. He F, Liu J, Zhu KD (2021) Optomechanical atomic force microscope. Nanotechnology 32(8):085505
65. Ando T et al (2005) High-speed Atomic Force Microscopy for Capturing Dynamic Behavior of Protein Molecules at Work. e-J Surf Sci Nanotechnol 3:384–392
66. Shimizu M et al (2022) An ultrafast piezoelectric Z-scanner with a resonance frequency above 1.1 MHz for high-speed atomic force microscopy. Rev Sci Instrum 93(1):013701
67. Watanabe H et al (2013) Wide-area scanner for high-speed atomic force microscopy. Rev Sci Instrum 84(5):053702
68. Uchihashi T et al (2016) Functional extension of high-speed AFM for wider biological applications. Ultramicroscopy 160:182–196
69. Schitter G et al (2007) Design and Modeling of a High-Speed AFM-Scanner. IEEE Trans Control Syst Technol 15(5):906–915
70. Kenton BJ, Leang KK (2012) Design and Control of a Three-Axis Serial-Kinematic High-Bandwidth Nanopositioner. IEEE/ASME Trans Mechatron 17(2):356–369
71. Yang C et al (2016) Design of a high-bandwidth tripod scanner for high speed atomic force microscopy. Scanning 38(6):889–900
72. Humphris ADL, Miles MJ, Hobbs JK (2005) A mechanical microscope: High-speed atomic force microscopy. Appl Phys Lett 86(3):034106
73. Picco LM et al (2007) Breaking the speed limit with atomic force microscopy. Nanotechnology 18(4):044030
74. Zhao B et al (2009) Large scan area high-speed atomic force microscopy using a resonant scanner. Rev Sci Instrum 80(9):093707
75. Fleming AJ (2009) A megahertz bandwidth dual amplifier for driving piezoelectric actuators and other highly capacitive loads. Rev Sci Instrum 80(10):104701
76. Wang X et al (2023) Stability Compensation Design and Analysis of a Piezoelectric Ceramic Driver with an Emitter Follower Stage. Micromachines (Basel) 14(5):914
77. Xu L et al (2021) The Application of Classical Control in the Design and Analysis of Power Amplifiers for Driving Piezoelectric Stack Actuators. Electronics 10(6):720
78. Comstock RH (1981) Charge control of piezoelectric actuators to reduce hysteresis effects. US
79. Main JA, Garcia E, Newton DV (1995) Precision position control of piezoelectric actuators using charge feedback. J Guid Control Dyn 18(5):1068–1073
80. Yi KA, Veillette RJ (2005) A charge controller for linear operation of a piezoelectric stack actuator. IEEE Trans Control Syst Technol 13(4):517–526
81. Fleming AJ, Moheimani SOR (2005) A grounded-load charge amplifier for reducing hysteresis in piezoelectric tube scanners. Rev Sci Instrum 76(7):073707
82. Yang C et al (2022) Comprehensive study of charge-based motion control for piezoelectric nanopositioners: Modeling, instrumentation and controller design. Mech Syst Signal Process 166:108477
83. Fleming AJ (2013) Charge drive with active DC stabilization for linearization of piezoelectric hysteresis. IEEE Trans Ultrason Ferroelectr Freq Control 60(8):1630–1637
84. Zhong J, Nishida R, Shinshi T (2021) A digital charge control strategy for reducing the hysteresis in piezoelectric actuators: Analysis, design, and implementation. Precis Eng 67:370–382
85. Huang L et al (2010) Switched capacitor charge pump reduces hysteresis of piezoelectric actuators over a large frequency range. Rev Sci Instrum 81(9):094701
86. Yang C, Li C, Zhao J (2017) A Nonlinear Charge Controller With Tunable Precision for Highly Linear Operation of Piezoelectric Stack Actuators. IEEE Trans Industr Electron 64(11):8618–8625
87. Yang C et al (2019) Charge Controller With Decoupled and Self-Compensating Configurations for Linear Operation of Piezoelectric Actuators in a Wide Bandwidth. IEEE Trans Industr Electron 66(7):5392–5402
88. Fleming AJ, Leang KK (2008) Charge drives for scanning probe microscope positioning stages. Ultramicroscopy 108(12):1551–1557
89. Yang C, Youcef-Toumi K (2022) Principle, implementation, and applications of charge control for piezo-actuated nanopositioners: A comprehensive review. Mech Syst Signal Process 171:108885
90. Kang S et al (2022) A Fractional-Order Normalized Bouc-Wen Model for Piezoelectric Hysteresis Nonlinearity. IEEE/ASME Trans Mechatron 27(1):126–136
91. Savoie M, Shan J (2022) Temperature-dependent asymmetric Prandtl-Ishlinskii hysteresis model for piezoelectric actuators. Smart Mater Struct 31(5):055022
92. Yang C et al (2021) Modeling and Control of Piezoelectric Hysteresis: A Polynomial-Based Fractional Order Disturbance Compensation Approach. IEEE Trans Industr Electron 68(4):3348–3358
93. Rakotondrabe M (2011) Bouc-Wen Modeling and Inverse Multiplicative Structure to Compensate Hysteresis Nonlinearity in Piezoelectric Actuators. IEEE Trans Autom Sci Eng 8(2):428–431
94. Yang C, Wang Y, Youcef-Toumi K (2021) Feedback-Assisted Feedforward Hysteresis Compensation: A Unified Approach and Applications to Piezoactuated Nanopositioners. IEEE Trans Industr Electron 68(11):11245–11254

95. Xiaobo T, Baras JS (2005) Adaptive identification and control of hysteresis in smart materials. IEEE Trans Autom Control 50(6):827–839
96. Hassani V, Tjahjowidodo T, Do TN (2014) A survey on hysteresis modeling, identification and control. Mech Syst Signal Process 49(1–2):209–233
97. Croft D, Shed G, Devasia S (2001) Creep, Hysteresis, and Vibration Compensation for Piezoactuators: Atomic Force Microscopy Application. J Dyn Syst Meas Contr 123(1):35–43
98. Croft D, Devasia S (1999) Vibration compensation for high speed scanning tunneling microscopy. Rev Sci Instrum 70(12):4600–4605
99. Rana MS, Pota HR, Petersen IR (2013) High-Speed AFM Image Scanning Using Observer-Based MPC-Notch Control. IEEE Trans Nanotechnol 12(2):246–254
100. Schitter G, Thurner PJ, Hansma PK (2008) Design and input-shaping control of a novel scanner for high-speed atomic force microscopy. Mechatronics 18(5–6):282–288
101. Nikooienejad N, Maroufi M, Moheimani SOR (2021) Iterative Learning Control for Video-Rate Atomic Force Microscopy. IEEE/ASME Trans Mechatron 26(4):2127–2138
102. Aridogan U, Shan Y, Leang KK (2009) Design and Analysis of Discrete-Time Repetitive Control for Scanning Probe Microscopes. J Dyn Syst Meas Control 131(6):061103
103. Wu J-W et al (2014) Design and Control of Phase-Detection Mode Atomic Force Microscopy for Reconstruction of Cell Contours in Three Dimensions. IEEE Trans Nanotechnol 13(4):639–649
104. Li L et al (2023) Periodic-Disturbance Observer Using Spectrum-Selection Filtering Scheme for Cross-Coupling Suppression in Atomic Force Microscopy. IEEE Trans Autom Sci Eng 20(3):2037–2048
105. Xie S, Ren J (2019) High-speed AFM imaging via iterative learning-based model predictive control. Mechatronics 57:86–94
106. Bazaei A, Yong YK, Moheimani SOR (2017) Combining Spiral Scanning and Internal Model Control for Sequential AFM Imaging at Video Rate. IEEE/ASME Trans Mechatron 22(1):371–380
107. Chuang N, Petersen IR, Pota HR (2013) Robust H∞Control in Fast Atomic Force Microscopy. Asian J Control 15(3):872–887
108. Leang KK, Zou Q, Devasia S (2009) Feedforward control of piezoactuators in atomic force microscope systems. IEEE Control Syst 29(1):70–82
109. Rana MS, Pota HR, Petersen IR (2017) Improvement in the Imaging Performance of Atomic Force Microscopy: A Survey. IEEE Trans Autom Sci Eng 14(2):1265–1285
110. Ren J, Zou Q (2014) High-speed adaptive contact-mode atomic force microscopy imaging with near-minimum-force. Rev Sci Instrum 85(7):073706
111. Swiadkowski B et al (2020) Near-zero contact force atomic force microscopy investigations using active electromagnetic cantilevers. Nanotechnology 31(42):425706
112. Lavanya SB, Jayanth GR (2022) Control of interaction force in constant-height contact mode atomic force microscopy. Mechatronics 88:102914
113. Fleming AJ (2010) Nanopositioning System With Force Feedback for High-Performance Tracking and Vibration Control. IEEE/ASME Trans Mechatron 15(3):433–447
114. Yang C, Youcef-Toumi K (2022) Decoupled tracking and damping control of piezo-actuated nanopositioner enabled by multimode charge sensing. Mech Syst Signal Process 173:109046
115. Mokaberi B, Requicha AAG (2008) Compensation of Scanner Creep and Hysteresis for AFM Nanomanipulation. IEEE Trans Autom Sci Eng 5(2):197–206
116. Fleming AJ, Kenton BJ, Leang KK (2010) Bridging the gap between conventional and video-speed scanning probe microscopes. Ultramicroscopy 110(9):1205–1214
117. Mahmood IA, Moheimani SOR, Bhikkaji B (2011) A New Scanning Method for Fast Atomic Force Microscopy. IEEE Trans Nanotechnol 10(2):203–216
118. Tuma T et al (2012) High-speed multiresolution scanning probe microscopy based on Lissajous scan trajectories. Nanotechnology 23(18):185501
119. Yong YK, Moheimani SO, Petersen IR (2010) High-speed cycloid-scan atomic force microscopy. Nanotechnology 21(36):365503
120. Nikooienejad N et al (2020) Video-Rate Non-Raster AFM Imaging With Cycloid Trajectory. IEEE Trans Control Syst Technol 28(2):436–447
121. Ziegler D et al (2017) Ideal Scan Path for High-Speed Atomic Force Microscopy. IEEE/ASME Trans Mechatron 22(1):381–391
122. Lee JS et al (2016) Multifunctional hydrogel nano-probes for atomic force microscopy. Nat Commun 7:11566
123. Coskun MB et al (2019) Q Control of an Active AFM Cantilever With Differential Sensing Configuration. IEEE Trans Control Syst Technol 27(5):2271–2278
124. Fairbairn MW, Moheimani SOR, Fleming AJ (2011) Q Control of an Atomic Force Microscope Microcantilever: A Sensorless Approach. J Microelectromech Syst 20(6):1372–1381
125. Kodera N et al (2010) Video imaging of walking myosin V by high-speed atomic force microscopy. Nature 468(7320):72–76
126. Ruppert MG et al (2016) A Kalman Filter for Amplitude Estimation in High-Speed Dynamic Mode Atomic Force Microscopy. IEEE Trans Control Syst Technol 24(1):276–284
127. Karvinen KS, Moheimani SO (2014) A high-bandwidth amplitude estimation technique for dynamic mode atomic force microscopy. Rev Sci Instrum 85(2):023707
128. Ragazzon MRP et al (2018) Lyapunov Estimator for High-Speed Demodulation in Dynamic Mode Atomic Force Microscopy. IEEE Trans Control Syst Technol 26(2):765–772
129. Fukuma T (2020) Improvements in fundamental performance of in-liquid frequency modulation atomic force microscopy. Microscopy (Oxf) 69(6):340–349
130. Miyata K, Fukuma T (2018) Quantitative comparison of wideband low-latency phase-locked loop circuit designs for high-speed frequency modulation atomic force microscopy. Beilstein J Nanotechnol 9:1844–1855
131. Mitani Y et al (2009) Wideband digital frequency detector with subtraction-based phase comparator for frequency modulation atomic force microscopy. Rev Sci Instrum 80(8):083705
132. Miyata K et al (2017) Dissolution Processes at Step Edges of Calcite in Water Investigated by High-Speed Frequency Modulation Atomic Force Microscopy and Simulation. Nano Lett 17(7):4083–4089
133. Yurtsever A et al (2022) Probing the Structural Details of Chitin Nanocrystal-Water Interfaces by Three-Dimensional Atomic Force Microscopy. Small Methods 6(9):e2200320
134. Park SW et al (1995) Nanometer scale lithography at high scanning speeds with the atomic force microscope using spin on glass. Appl Phys Lett 67(16):2415–2417
135. Szoszkiewicz R et al (2007) High-speed, sub-15 nm feature size thermochemical nanolithography. Nano Lett 7(4):1064–1069
136. Vicary JA, Miles MJ (2009) Real-time nanofabrication with high-speed atomic force microscopy. Nanotechnology 20(9):095302
137. Chen C et al (2015) Construction of 3D polymer brushes by dip-pen nanodisplacement lithography: understanding the molecular displacement for ultrafine and high-speed patterning. Small 11(5):613–621
138. Yao B et al (2022) Surfing Scanning Probe Nanolithography at Meters Per Second. Nano Lett 22(6):2187–2193
139. Vettiger P et al (2000) The "Millipede"—More than thousand tips for future AFM storage. IBM J Res Dev 44(3):323–340
140. Ivanova K et al (2008) Scanning proximal probes for parallel imaging and lithography. J Vac Sci Technol B 26(6):2367–2373
141. Holz M et al (2018) Field-emission scanning probe lithography tool for 150 mm wafer. J Vac Sci Technol B Nanotechnolo Microelectron: Materials, Processing, Measurement, and Phenomena. 36(6)
142. Minne SC et al (1998) Centimeter scale atomic force microscope imaging and lithography. Appl Phys Lett 73(12):1742–1744
143. Pozidis H et al (2004) Demonstration of Thermomechanical Recording at 641 Gbit/in^2. IEEE Trans Magn 40(4):2531–2536
144. Kaestner M, Rangelow IW (2020) Scanning probe lithography on calixarene towards single-digit nanometer fabrication. Intern J Extreme Manuf 2(3):032005
145. Dai G, Zhu F, Fluegge J (2015) High-speed metrological large range AFM. Measurement Science and Technology 26(9):095402
146. Dai G et al (2018) Fast and accurate: high-speed metrological large-range AFM for surface and nanometrology. Meas Sci Technol 29(5):054012

147. Klapetek P et al (2015) Large area high-speed metrology SPM system. Nanotechnology 26(6):065501
148. Heaps E et al (2020) Bringing real-time traceability to high-speed atomic force microscopy. Meas Sci Technol 31(7):074005
149. Zhang T et al (2022) Correlative AFM and Scanning Microlens Microscopy for Time-Efficient Multiscale Imaging. Adv Sci (Weinh) 9(12):e2103902
150. Cao W et al (2021) Massively parallel cantilever-free atomic force microscopy. Nat Commun 12(1):393
151. Kim G et al (2022) Binary-state scanning probe microscopy for parallel imaging. Nat Commun 13(1):1438
152. Strahlendorff T et al (2019) Tip wear and tip breakage in high-speed atomic force microscopes. Ultramicroscopy 201:28–37
153. Paul PC et al (2011) Rapid turnaround scanning probe nanolithography. Nanotechnology 22(27):275306
154. Yang C et al (2017) Probing the Morphology and Evolving Dynamics of 3D Printed Nanostructures Using High-Speed Atomic Force Microscopy. ACS Appl Mater Interfaces 9(29):24456–24461
155. Angelov T et al (2016) Six-axis AFM in SEM with self-sensing and self-transduced cantilever for high speed analysis and nanolithography.J Vac Sci Technol B Nanotechnol Microelectron: Materials, Processing, Measurement, and Phenomena. 34(6)
156. Holz M et al (2019) Correlative Microscopy and Nanofabrication with AFM Integrated with SEM. Microscopy Today 27(6):24–30
157. Hofmann M et al (2019) Nanoscale lift-off process using field emission scanning probe lithography. J Vac Sci Technol B Nanotechnol Microelectron: Materials, Processing, Measurement, and Phenomena 37(6):061803
158. Rangelow, I.W., et al., Atomic force microscope integrated with a scanning electron microscope for correlative nanofabrication and microscopy. Journal of Vacuum Science & Technology B, Nanotechnology and Microelectronics: Materials, Processing, Measurement, and Phenomena, 2018. 36(6)
159. Kreith J et al (2017) A versatile atomic force microscope integrated with a scanning electron microscope. Rev Sci Instrum 88(5):053704
160. Andany SH et al (2020) An atomic force microscope integrated with a helium ion microscope for correlative nanoscale characterization. Beilstein J Nanotechnol 11:1272–1279
161. Iwata F et al (2013) Development of nanomanipulator using a high-speed atomic force microscope coupled with a haptic device. Ultramicroscopy 133:88–94
162. Yao T-F, Duenner A, Cullinan M (2017) In-line metrology of nanoscale features in semiconductor manufacturing systems. Precis Eng 47:147–157
163. Kohli P et al (2011) High-speed atmospheric imaging of semiconductor wafers using rapid probe microscopy, in Metrology, Inspection, and Process Control for Microlithography XXV
164. Yao T-F, Connolly LG, Cullinan M (2019) Expanded area metrology for tip-based wafer inspection in the nanomanufacturing of electronic devices. J Micro/Nanolithogr MEMS MOEMS 18(03):034003
165. Cain JP et al (2015) High-speed AFM for 1x node metrology and inspection: Does it damage the features?, in Metrology, Inspection, and Process Control for Microlithography XXIX

Publisher's Note

Springer Nature remains neutral with regard to jurisdictional claims in published maps and institutional affiliations.